Laser Stabilization and Linewidth Narrowing for Molecular Spectroscopy

Lukas Song

Advisor: Professor David Hanneke
May 9, 2024

Submitted to the
Department of Physics & Astronomy of Amherst College
in partial fulfillment of the
requirements for the degree of
Bachelors of Arts with honors

Abstract

An optical clock is a clock that utilizes monochromatic light to serve as the oscillator. Due to their extremely high oscillation frequency, optical clocks are candidates for high precision clocks. Recently, many experiments try to incorporate these clocks to measure transition between states of atoms and molecules to great precision, allowing us to search for changes in fundamental constants over time, in order to test models beyond standard physics. Our lab will incorporate a molecular oxygen ion within a Paul trap and excite its sixteenth vibrational mode through two photon transitions to measure these changes. This thesis is the implementation of the laser source necessary to drive the two photon interaction. I have incorporated a high finesse cavity to lock the laser to, allowing us to drop the laser linewidth down from 200 kHz all the way to 2.2 kHz which will give us a precision of $\frac{\Delta\mu}{\mu} = 6.8 \times 10^{-12}$. This will serve as an excellent stepping stone to get lock onto the ultra high finesse cavity which will narrow its linewidth an order of magnitude more.

Acknowledgments

I would like to thank Professor Hanneke for patiently guiding me through this experiment, Ambesh Singh and Michael Mitchell for helping me within the lab, Brian Crepeau and Jim Kubasek for assisting me with the electronics and hardware chassis, and my friends and family for morally supporting me throughout this project. I would also like to thank the NSF foundation for allowing this funding to happen in the first place. This thesis is based upon work supported by the Amherst College Provost and Dean of the Faculty and by the National Science Foundation under grants PHY-2207623 (RUI PM) and PHY-1806223 (RUI)

Contents

List of Figures

Chapter 1

Introduction

1.1 Optical Clocks

Clock is an instrument that is used to measure time. Although a clock may seem like a limited measurement device, its versatility is, at times, astonishing. Historically, accurate clocks have been utilized to measure the longitude of the Earth, and the invention of an accurate, robust watch has revolutionized marine navigation. Today, an atomic clock operates within a satellite to precisely time GPS signals, allowing us to use the miniscule time differences between the satellites to triangulate the signal to a precise location.

Despite that, we nearly never think of the theory behind the clocks, so what drives a clock and how does it work? The simplest clock is driven by an oscillator with a stable reference. In our day to day basis, it would be a quartz crystal cut to oscillate at a specific frequency, typically at 32,768 Hz, which then is measured against an electronic oscillator which tunes itself against the crystal, from there, digital and analog processing is done to turn that oscillation into the seconds we know and love [1]. However, quartz crystal will not work for cases like GPS where we are trying to triangulate to a point, with a 32 kHz cycle giving us a clock uncertainty of 10^{-4} s/day

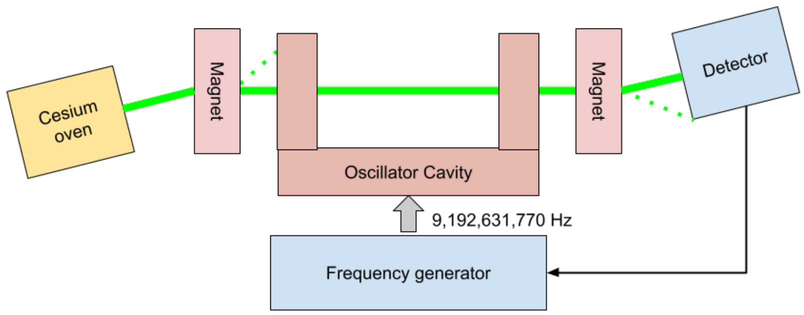

Figure 1.1: The cesium clock functions by expelling cesium atoms from an oven which heats them, then is sent to a magnet to pick and and collimate the beam into one, then the ions are sent on an oscillator cavity and placed into a magnet to pick out and collimate the expelled atoms which is sent to a detector [2].

[2] would mean that we would be off by 30 km by the end of the day, rendering it nearly useless. So we would need a better clock, to do that, we can utilize an atomic clock, which would use a microwave oscillator with cesium atom. The process of doing that would be to isolate the correct states of cesium atom by using a Stern Gerlach magnet (or through an inhomogeneous field) which will isolate the correct spin of the cesium atom. The corrected and "collimated" cesium atoms would then be sent to an oscillating, magnetic field within a cavity which, if tuned to the atomic resonant frequency, will then exit the cavity, and collimated with an magnet once more before being sent to the detector. The details of a cesium clock is illustrated in figure 1.1. So, within the case of cesium clocks, the oscillator is the tunable, electronic oscillator driving the cavity's magnetic field, and the reference would be the magnetic transition within the cesium atom. Since the electrons in atoms have fixed transitions due to Quantum Mechanical effects, this transition frequency is fixed, thereby serving as a stable reference point.

The the cavity frequency will be tuned to resonance by finding the point of maximum number of transitions detected by the detector. By changing the frequency of the oscillations, we can get a stable, electrical oscillations to connect to a clock

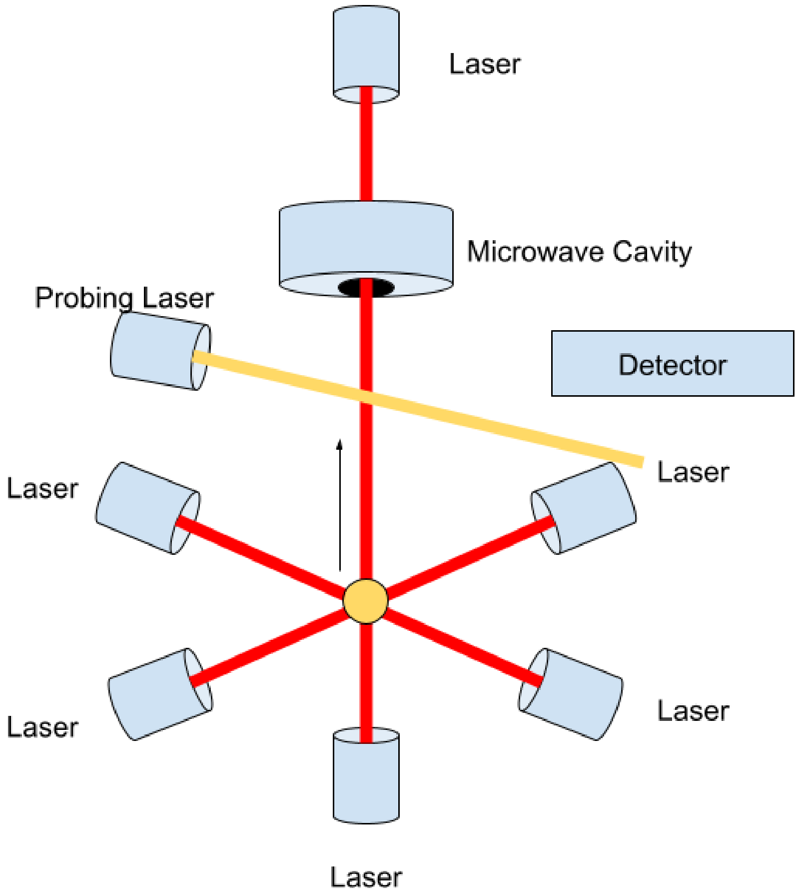

Figure 1.2: The cesium fountain clock works by first cooling the cesium with the cooling lasers, then detuning the vertical lasers to send it upwards, then the particles go up through the microwave resonator, then fall down back then where it gets detected with another laser.

circuit. However, this method will not be precise enough as the temperature of the atoms induce doppler broadening, which will limit the resolution of the clock we can go all the way down.

To account for that, another method of cesium atom clocks were made known as the cesium fountain clock was made. The fountain clock operates by utilizing a lasers to cool the cesium atoms down all the way down to 6 μK, which will then be detuned upwards (against gravity) to a set velocity (typically 4 m/s), which will then be sent through the microwave cavity to excite the ions to a new state, before it falls back

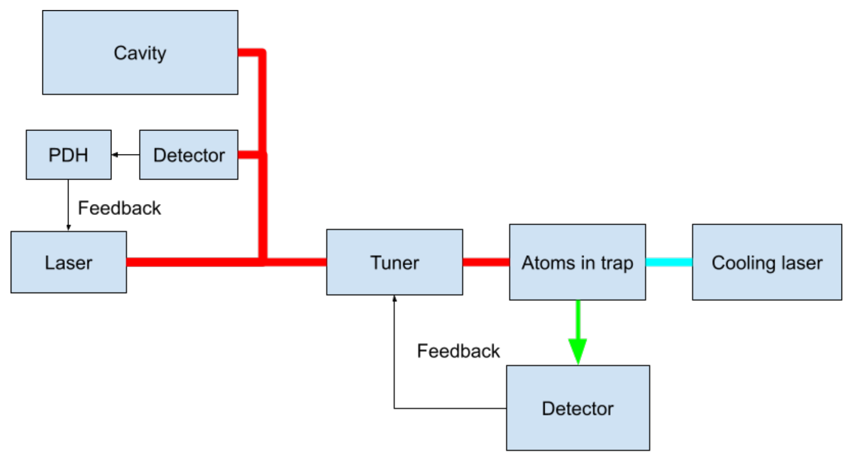

Figure 1.3: The typical optical clock functions by locking itself to a stable reference (a stable optical cavity), then it tunes around using an AOM, where it would go on a feedback loop to find the point of maximum of the atomic transition, where it will lock itself onto it. However, as our system require a larger range, AOM proves to be impractical.

down through the cavity and will then be detected with a detector [2]. With the detector, we can tune the microwave cavity frequency to maximize the transition. By doing that, we can go down from the accuracy of 10^9 to 10^{13} [2].

$$\sigma \propto \frac{\Delta v}{v_0} \frac{1}{SNR} \tag{1.1}$$

[2]

However, the leading edge of today would be to utilize optical oscillator to be our oscillation for the clock. As referenced in figure 1.3, optical clock utilizes light to be the oscillator instead. Since the stability of the clock is inversely proportional to the frequency of the oscillator from equation 1.1, so a precision optical clock would be better for measurement.

By utilizing an optical clock, it would allow us to measure the changes in frequency to a much higher precision, due to its extremely high stability given to the optical clock itself.

1.2 Beyond the Standard Model

The standard model describes many parts of physical phenomena within our universe; however, there are parts, namely Dark Matter, that is not explained by it at all.

One of the theories that may explain such phenomena would involve a new particle that would act as a massive, scalar field over space. The massive field will interact with the fundamental constants, leading us to have changes in fundamental constants over long periods of time [3]. This is significant as the standard model describes the fundamental particles and in no place indicates of any changes being made to these fundamental properties. So, the model of having a massive, scaler field all over space would be significant since it would have to deal with matters — protons and neutrons has its mass dominated by strong forces between quarks and gluons against electrons, which is an elementary particle. Due to that, any changes in these fundamental constants can potentially insinuate new physics!

To check that, one can examine some nice, measurable ratios and those are α which is the fine-structure constant that characterizes the electromagnetic interactions of charged particles, and μ which is the ratio between the mass of a proton and an electron. These two pop off frequently as these would be utilized in many calculations interacting with real particles since our real particles are quantum mechanical systems of protons and electrons.

The ratio $\dot{\mu}/\mu$ can be measured in many different ways. For example, through the cesium clock method, the smallest we have gone down to is $\dot{\mu}/\mu = -0.8 \pm 3.6 \times 10^{-17} yr^{-1}$ [4]. Alternatively, the lowest achieved with a comparison of two molecular transitions to get the values $\dot{\mu}/\mu = -0.3 \pm 0.1 \times 10^{-14} yr^{-1}$ [5] instead.

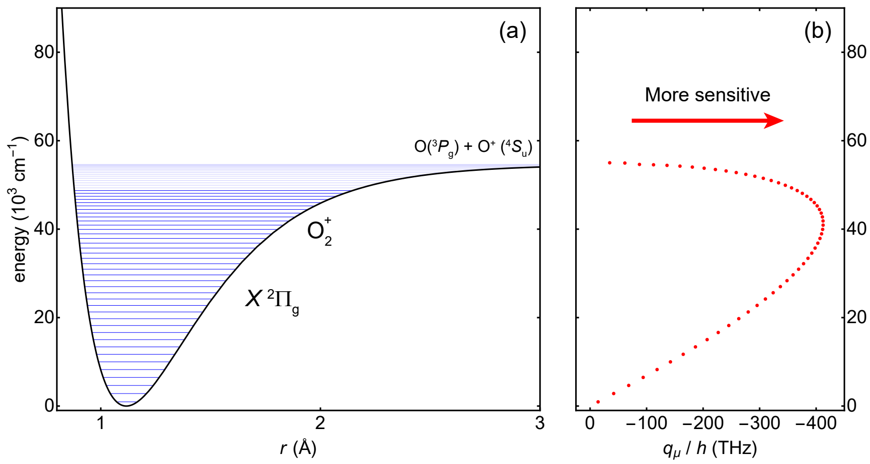

Figure 1.4: The oxygen ion transition and its sensitivity to μ plotted onto a graph. Used with permission from reference [6]

1.3 Our Experiment

1.3.1 Molecular Oxygen Ions and Paul Trap

The reference within our case would be an diatomic oxygen ion, which, as shown within the paper [6], has a remarkable amount of sensitivity for detecting these changes in μ. Due to that, it would serve as an excellent transition to look for these changes despite the fact that we would probably not be able to generate an optical clock as stable as some of the papers mentioned above. The sensitivity of the relates by the following equation:

$$\frac{\Delta\mu}{\mu} = q_\mu \frac{\Delta f}{f} = \frac{\Delta f}{f_\mu} \tag{1.2}$$

The sensitivity, as illustrated in figure 1.4, relates with the equation 1.2, to measure the μ value. By having a much higher sensitivity, it would allow us to utilize get better μ precision even with a less precise clock. This effect stems from the fact that oxygen is a diatomic molecule, which has an anharmonic potential. The anharmonic potential can be perturbed from the quantum harmonic oscillators, which depends on μ, thereby giving us the element that is highly sensitive to μ. For more details, please check Hartman's thesis [7]. To accomplish the measurement with any high precision, we would have to account for the Doppler shifting by cooling down the laser significantly, akin to how the fountain cesium clock has been done. As we would be doing these experiments with many atoms other than the molecular oxygen ion, a standard cooling setup of incorporating six lasers to cool the atom is not practical. For that, the labs has incorporated a linear paul trap to limit the movement of the ions, which will afterwards be cooled by a cooling laser at direction that projects onto each axis, thereby allowing us to cool all three directions simultaneously [8]. Furthermore, the trapping, as the name indicates, traps the ions into place, allowing us to probe at the ions for longer periods of time. By being freed to incorporate just a single laser for cooling, we can effectively switch between many lasers and ions, allowing us to do this experiment on a tabletop setting readily. Moreover, oxygen is cheap, easy to use, and its relatively easy to handle as well, making it ideal for a laboratory setup like ours. However, while diatomic oxygen ions serve as an excellent molecule to check for μ, the molecule has no effective lasers suitable for allowing it to cool down [9], forcing us to utilize a different method of cooling. Therefore, the beryllium ions, as shown and explored in [10], has been utilized as our candidate for sympathetically cooling down the oxygen ions. Since, within the trap, the ions are crystallized, we would have the particles interacting with one another through Coulomb forces. So by cooling down the movement of the beryllium ions, we can cool down the oxygen molecules as well. The exact analysis and simulations are currently being conducted by Michael Mitchell, which will be reported hopefully soon.

Pairing the optical clock along with the increased sensitivity will make this transition be a prime candidate. For that though, I would have to setup an optical clock system to conduct this experiment. The chosen vibrational transition was v=16; however, due to the fact that there is a moderate uncertainty present in the transition

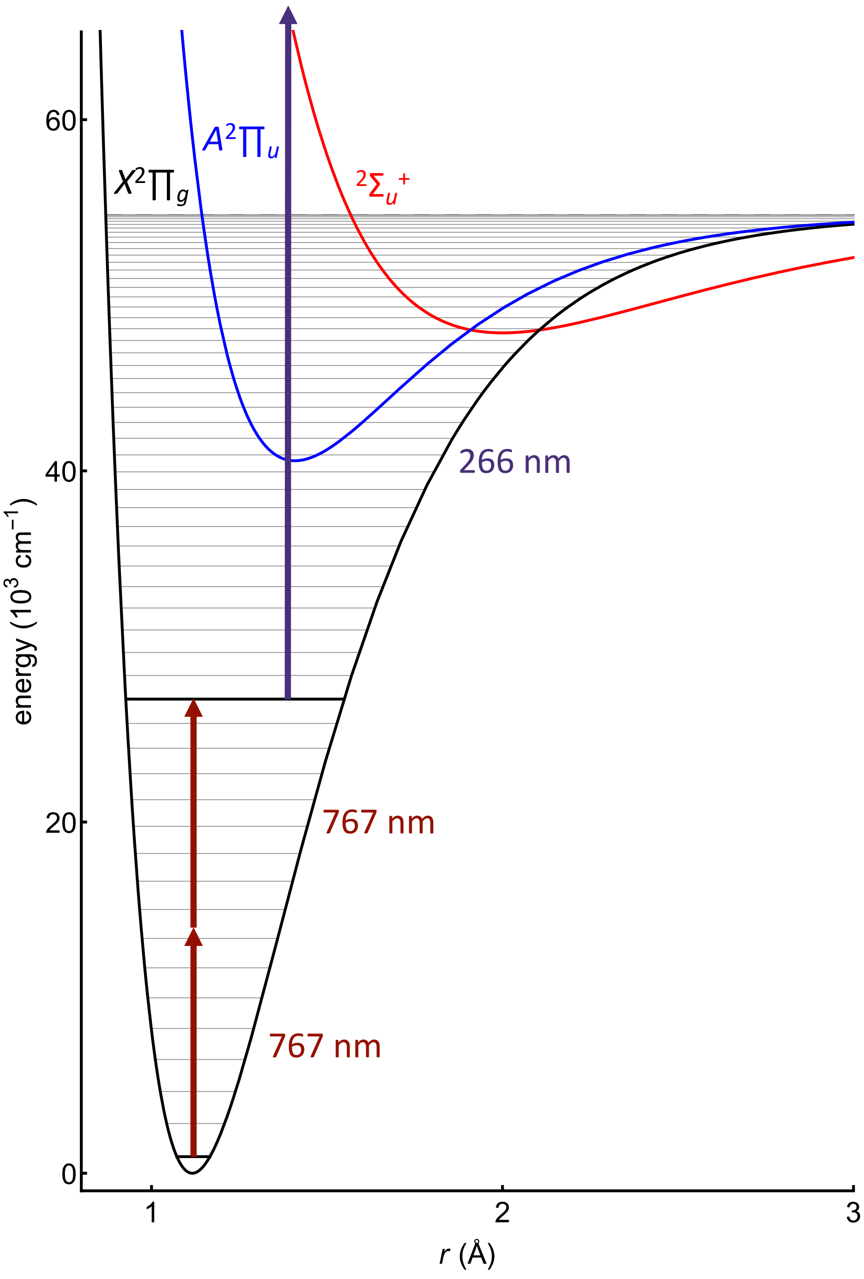

Figure 1.5: The transitions of molecular oxygen ion on how it reaches dissociation. Used with permission from reference [7]

frequency, we would need a wider range of tunability. So the standard method of independent tuning to setup the optical clock will not work for our case. The stabilized tunable laser will also have to be much brighter than this since the transition from ground state of molecular oxygen ion to v=16 will be undergoing a two-photon transition, which will be a nonlinear transition and be more favorable with more electric field. The two state transition will be nonlinear since it would be dependent on photon density, which is dependent on the square of the electric field. As shown in 1.5, we can observe that not only will be bring the oxygen ions up to a vibration state v=16, we would also have to dissociate it with a UV laser to dissociate the molecule and choose that as our probing point as well. Thankfully, this has been done beforehand by Addison's work [7]. Later on, the people after me will have to use the optical clock to measure the transition frequency the vibrational state of oxygen ion over long stretches of time, measure the μ then will have to model the changes ultimately.

Chapter 2

Laser Operations and Sources of Noise

Since lasers are crucial since it would be the oscillator for our clock, one has to ask, what exactly is a laser and how does it work? By looking into the theory behind the operations of laser and the potential noise sources we would have to worry about, we can try to fix these issues to try and get a better oscillator.

2.1 What is a Laser?

A laser is an acronym for Light Amplification by Stimulated Emission of Radiation, which describes a collection of devices where it amplifies or generates coherent light. Light here is defined as an Electromagnetic wave that is in the infrared, visible, or Ultraviolet regime. Other electromagnetic wave amplification systems are present as well (namely microwave or X-rays), but such will not be discussed within this paper.

Stimulated emission is a type of optical emissions caused by an excited electron interacting with a photon with exactly its band-gap energy causing it to drop down to a lower energy state with the energy being outputted as another photon of the same phase, frequency, and polarization as shown in figure 2.1.

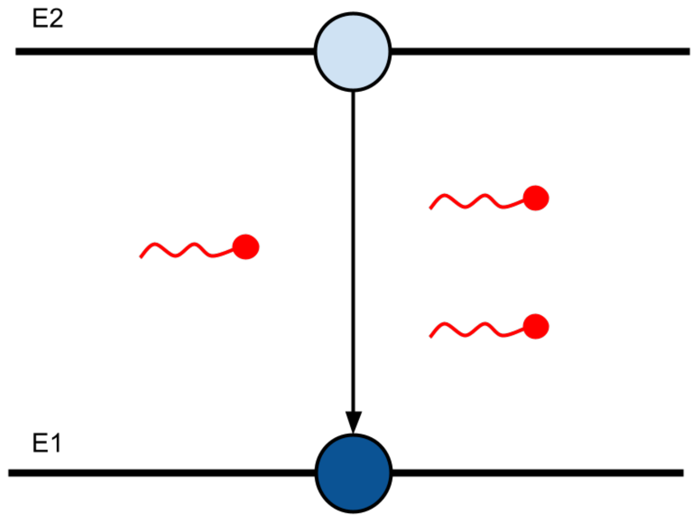

Figure 2.1: Stimulated Emission of an electron going from higher to lower energy

Due to the fact that stimulated emission generates one more photon than it started with, we can maintain this chain reaction for a significant laser gain if we were to maintain a high population of excited electrons in our system. This action of getting electrons from a lower energy state to a higher energy state so that more are populated in the higher energy state is called population inversion. The method of obtaining said population inversion would heavily depend on the medium that is generating the light as well. However, as with any systems, we would also be subject to spontaneous emissions, or the electron emitting light and going down in energy spontaneously. This would be undesirable as this would mean that our photon generation would be spurious and uncontrolled, which would hinder us in getting a coherent light source. Furthermore, it would make the medium more efficient if we were to reuse some of the photons that escaped the system, we can add additional mirrors to try and catch it back and send it back to the medium instead, as shown in figure 2.2. The lasers will begin as a spontaneous emission, where it would be caught into a specific geometric pattern until it reaches the lasing threshold, where the optical gain by the stimulated emission will carry on with the light production as long as population inversion is

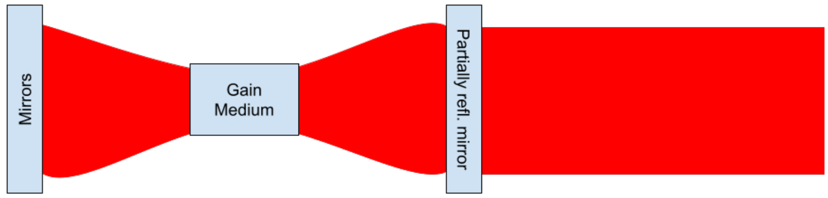

Figure 2.2: The image depicts a laser medium that is surrounded by a pair of mirrors, creating an optical cavity.

maintained.

The optical cavity that has been created by these two mirrors, which, not only would it allow us to maintain a higher level of photons present within the system, would also allow the light to be constrained to a specific geometry. With our new specified optical geometry, it would allow us to combat against spontaneous emissions which doesn't have any directional preference differing from the controlled directionality of photons generated by stimulated emissions. Thanks to that, we now have the light spatially coherent as well. While lasers work like these in the most basic sense of operation, its exact method of photon generation and amplification would determine what would be the best performance we can get from our laser.

2.2 Diode laser

2.2.1 Operation

For our particular example, the population inversion is obtained through an electrical current through a semiconductor diode. The laser diode is produced from slightly modifying a conventional light emitting diode — that being changing the structure of the diode so that all of the recombination occurs in a specific region, as shown in 2.4. Unlike a conventional light emitting diode, a laser diode will have some other layer, typically an undoped layer, to be the active region [11].

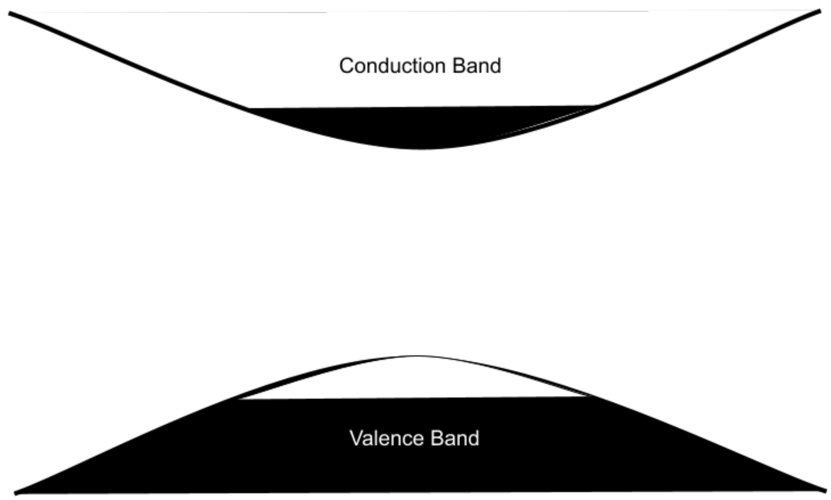

Figure 2.3: Bandgap of a semiconductor, the valence band on the bottom and the conduction band on top forces the electrons to be separated in two discrete regions. This energy gap would allow us to generate a photon.

The population inversion of the electron occurs due to the current being fed into the diode. and the cavity would be from the active layer, which is typically undoped semiconductor, between the doped semiconductors with a reflective and a partially reflective layer applied on each side to serve as an optical cavity.

However, this is going to yield a non-ideal laser as the geometry of the light output would not be a simple, Gaussian output, but an elliptical output instead (we can either trim it with a fiber or use a cylindrical lens to squish it back to Gaussian), and the linewidth of the output light would be larger than most other lasers as the semiconductors force us to a wider linewidth due to the wider range of energy gaps are allowed.

For more details regarding semiconductor lasers, please consult Nagourney's book [11] and Fundamentals of Photonics [12].

Due to that, the laser will have an additional optical setup to both get a more workable output geometry (a simple gaussian beam) and a finer, tuneable linewidth through a diffraction grating will help us get a better optical clock. As this would

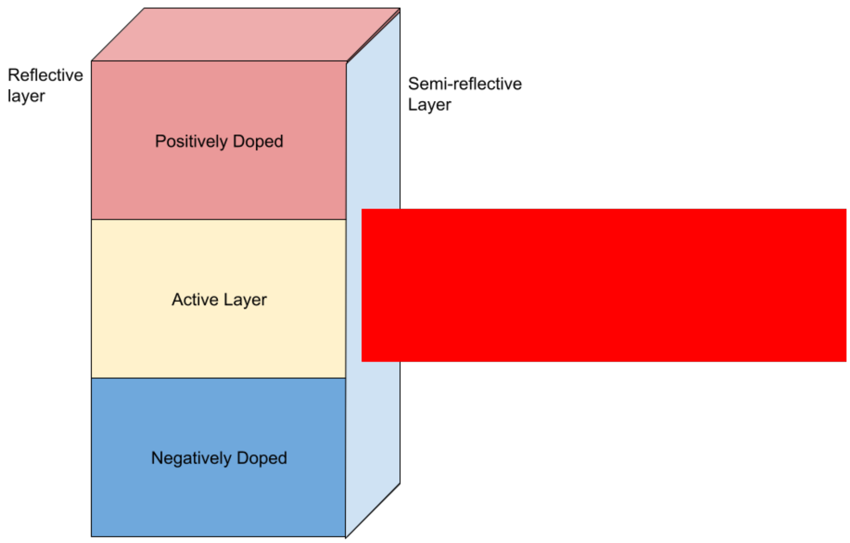

Figure 2.4: The illustration shows the basic laser diode, it is a diode with an active, undoped region, where stimulated emission and recombination of electrons and holes will occur and the cavity is that region with both sides covered with a reflective coating instead.

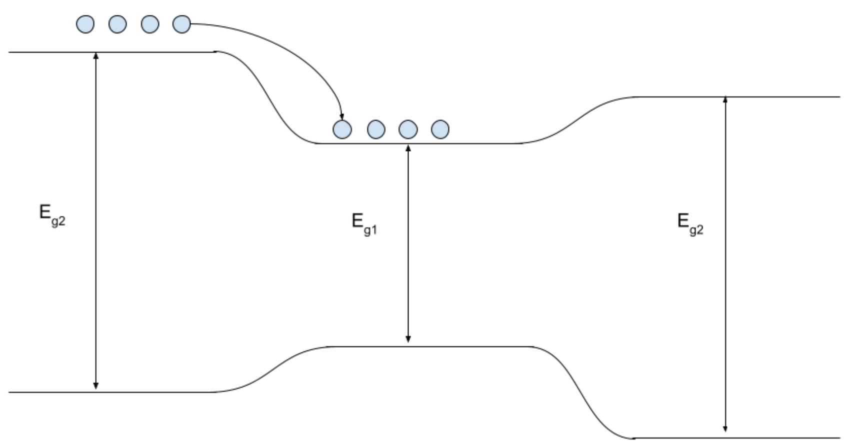

Figure 2.5: Unlike a conventional diode, the laser diode also adds an active, undoped region and the effects are shown within the diagram. By adding this region, we now have a geometric region where most of stimulated emissions can occur, rather than making it rely on difficult to control effects like drifts and diffusions. E_{g1} is the energy gap caused by the two doped regions (positive and negative) while E_{g2} is the energy gap of the active region. [11]

not only introduce us to a clock that we can match to a specific resonance, we would also narrow the linewidth further down as well.

However, we know that, due to various processes, the laser will be impacted by further noise sources, which will broaden the linewidth of the laser and impart drift to the frequency of the laser as well, making it a poor oscillator for the optical clock.

2.2.2 Noise

Since we have used a current source and a diffraction grating to both drive and turn the laser diode into a single mode output, the noises from these two will write onto our laser frequency noise as well. The primary sources of frequency noise would be through the piezo creep of the diffraction grating (slow noise) and the current noise being applied through the laser as well (fast noise). While under normal conditions, temperature of the laser medium/piezo and vibrations of the diffraction grating would play a significant role, since we are utilizing a pre-manufactured product that is engineered around these problems, we won't have to focus on that too much in our case. The creep becomes frequency noise by changing the piezo dimension, which changes the angle in which the diffraction grating reflects the light, which will correspond to a frequency change.

The equations for the piezo/grating setup illustrated at figure 2.6 would be the standard diffraction grating formula which is

$$d \sin(\theta) = m\lambda \tag{2.1}$$

Here d is the distance between the gratings and λ is the wavelength of the light. By looking at our $m = 1$ solution, we now get:

$$\theta = \sin^{-1} \frac{c}{\nu d} \tag{2.2}$$

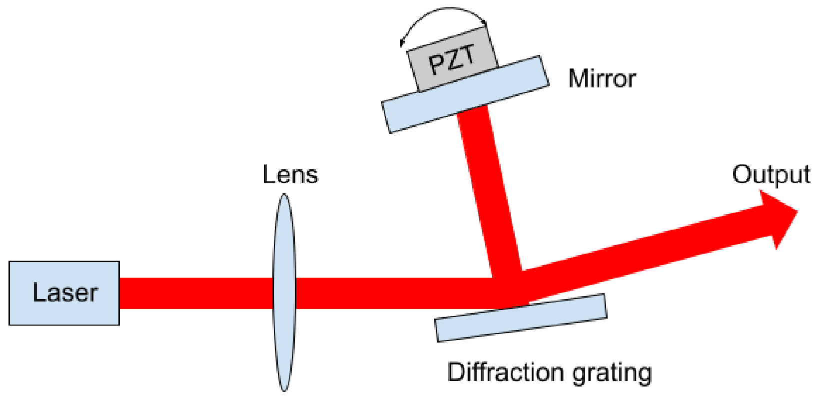

Figure 2.6: The diffraction grating and the tunable mirror will create an external cavity, which would, if tuned properly, help us extract a single mode out of the laser. Furthermore, since the diffraction grating also has an angle/wavelength relation, we can also tune what our output laser frequency would be with ease. The piezo crystal will alter the angle of the mirror since once side would be fixed, while the other side would be changing in length, this would allow us to resonate with a different angular output of the diffraction grating.

So we have now converted the frequency spread of the light input into a controllable angle separation which we can use to create another optical cavity (external cavity portion of ECDL or External Cavity Diode Laser). This external cavity, with its narrower linewidth and tunability, would allow us to rotate around until we can create a stable, single-mode laser light. Not only would it help us with the linewidth, we can also tune the output wavelength by rotating the diffraction grating up to a certain point (changing the current to ensure that the laser cavity will also track along helps ensure that we won't mode hop). However, this would mean that with the piezo controlling the angle that is selected from the diffraction grating, the piezo creep will now translate to angle change, which would give us the drift in frequency. This tends to be slow as a piezo-mirror setup is relatively massive and effects of piezo creep occur in long time-spans.

The current noise imparts into the frequency noise due to the fact that the index of refraction of the semiconductor depends on the current that is flowed through it

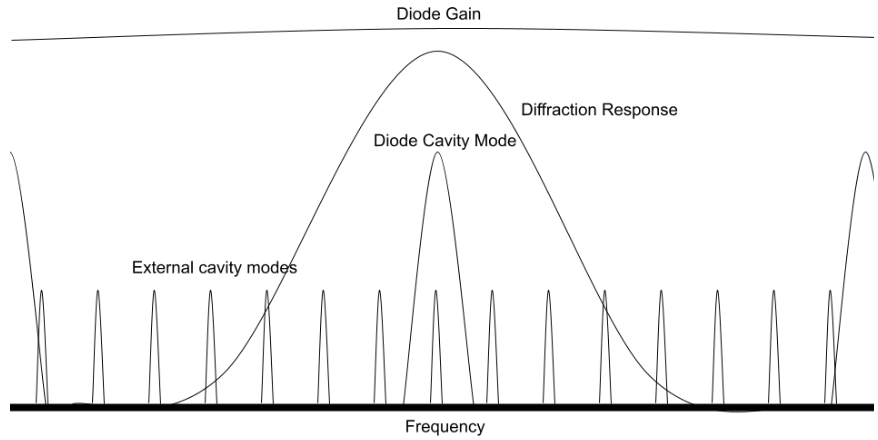

Figure 2.7: Laser gain is set by the diode itself, but the diffraction response and the external cavity is controlled by the diffraction grating and the laser cavity is controlled by the laser temperature and the current. The actual gain would be product of all of these gains.

[11]; therefore, the frequency noise becomes index of refraction noise which becomes a frequency noise as it is changing the optical cavity of the laser itself. This effect stems from the fact that increased current increases the total population of electron and hole pair within the diode and with more of these pairs being present, the light will have to move slower through the medium as it has more objects it must interact with in order to traverse.

As mentioned earlier in figure 2.2 and in figure 2.4, we can see that the two reflective surfaces made on both sides of the diode will create an optical cavity with the diode length being the separation distance between the two mirrors as well, so light will resonate at frequencies of the following equation:

$$f = \frac{mc}{2dn} \tag{2.3}$$

Where m is a positive integer d is the length of the diode, and n is the index of refraction of the diode; if assuming visible light with tiny diodes (about 1 mm or smaller), we can expect m to be around 10,000 [13] [14]. Due to that, through changes in the diode length (this can occur with temperature changes) or changes in the index of refraction can cause a change in the resonant frequency of the external cavity as well.

While the changes of the index of refraction are relatively small, with the optical cavity being much longer than the wavelength of light itself, the changes due to the index of refraction would be relatively noticeable in terms of the change in frequency; the typical amounts of changes due to current changes would be approximately 0.1 GHz/mA [11]; however, this will depend on the laser diode parameters significantly (the diode material and the dimensions of the diode as well).

So, the laser linewidth will be broadened and will drift over time, making it a poor oscillator to make a stable optical clock with. Therefore, we would have to introduce active methods to control and stabilize the laser even further than this. One way to deal with both the linewidth broadening and the drift would be through setting the laser to be locked onto an optical resonator that is more stable than the laser itself. Then, we can now get the laser locked on and serve as an excellent oscillator.

Chapter 3

Theory

Within the field of physics, there are many models to try and explain some things beyond the standard model, one of the ways to test that is to analyze the proton to electron ratio, μ, over long time periods. To do that, many different methods have been proposed from the largest astronomical measurements to the smallest ion measurements. The experiment presented here requires us to look very closely into O_2^+ transitions to analyze the ratio since the diatomic molecule can be modeled as an anharmonic resonator which allows us to observe the phenomena to a greater sensitivity. Prior to that, an ion trap has been made and improved in previous theses to reduce the movement of the ion, allowing us to reduce the doppler shift and look at these transitions to greater details. However that also entails our need for a more precise optical clock to help us analyze the transition in greater detail than before. This thesis will deal with methods to try to make a tuneable optical clock to help us analyze the transition.

While some laser pre-stabilization has been done through an adjustable cavity, it is still susceptible to the current noise applied to it; therefore, we must find an optical reference far more stable than the laser itself to lock onto in order to improve the laser performance that we can get. Due to the setup of the system itself, the fundamental limit in noise that we can approach would be the shot-noise from the detector, but that goes beyond the what we need in our case so this method will work for our purpose.

3.1 Theory

The molecular ion of O_2^+ is a simple diatomic ion of two oxygen atoms bound together. Due to that, we can model the transitions of the oxygen as an anharmonic oscillator as we can model it as two weights connected by a spring to model its vibrational modes. The vibrational modes of the oxygen, which allows us to look into μ with greater sensitivity, allows us to set up a reference for our optical clock.

3.2 Fabry Perot Interferometer

3.2.1 Axial Modes and Finesse

While a general summary of fabry perot cavity characteristics are detailed below, to see a better reference, please consult Siegman's Laser book. Fabry Perot cavity is an optical cavity of two mirrors separated with a predetermined distance, and with the resonator being a standing wave, resonance, the frequency separation between the axial modes of the cavity will be characterized as

$$FSR = \frac{c}{2L} \tag{3.1}$$

Where the FSR means the free spectral range which is the spacing between its axial modes and L being the length of the resonator. To model how the light interact with the fabry perot cavity, we must look at what happens to it as it goes in and reflects within the cavity. When we observe at how the individual light waves enter and interact within the cavity, we observe that the all of the reflected lights will have an additional optical distance of odd multiple of the cavity length added into it (with the transmission having an even multiple of cavity length added within instead).

$$F_{reflection} = \frac{r(1 - e^{i\omega/FSR})}{1 - r^2 e^{\frac{i\omega}{FSR}}} \tag{3.2}$$

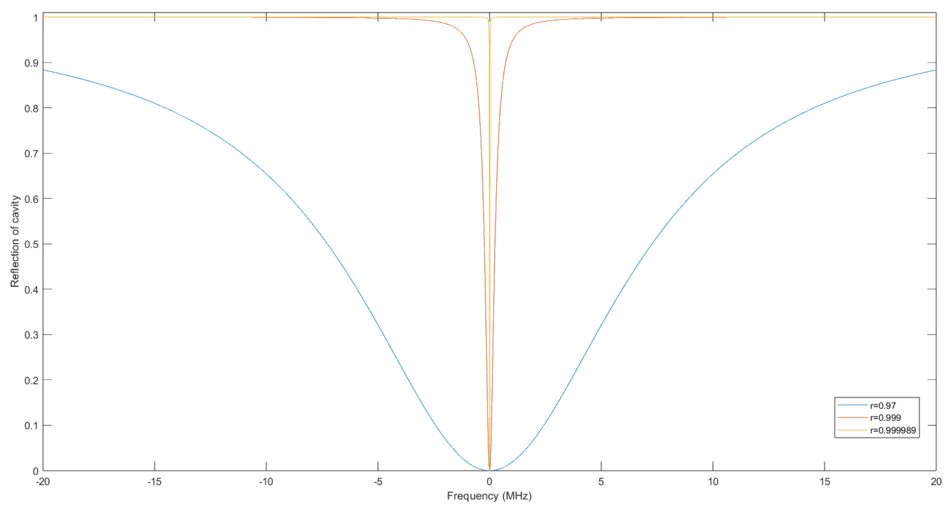

Figure 3.1: Y-axis is reflectivity and the x-axis is in MHz. These are simulated results for the cavities we will incorporate later on.

As viewed above, the reflectivity of the mirrors of the cavity reduces the linewidth of the resonating frequencies for the cavity. A similar relation is witnessed for the transmission as well. Utilizing similar methods of calculation, we can also gather similar equation for the transmission as well:

$$F_{transmission} = \frac{(1 - r)(1 + re^{i\omega/FSR})}{1 - r^2 e^{\frac{i\omega}{FSR}}} \tag{3.3}$$

Here, with the linewidth being lorentzian, we can calculate the linewidth of the resonance. Utilizing the Lorentzian linewidth, we can now calculate the finesse of the cavity by defining the finesse to be a ratio of the FSR of the cavity with the linewidth.

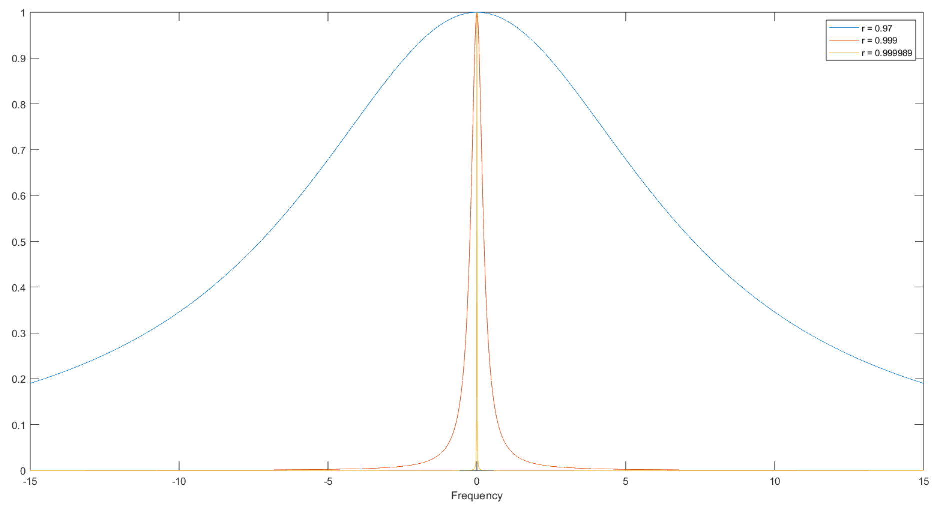

Figure 3.2: Y-axis is transmission and the x-axis is frequency in MHz. These results are also the cavity we would be incorporating later on.

This equation, after much algebra, simplifies to a neat relation of the following:

$$Finesse = \frac{\Delta\nu_{FSR}}{\Delta\nu_{linewidth}} = \frac{\pi r}{1 - r^2} \tag{3.4}$$

By utilizing the reflectivity of the mirrors of the cavity and the length itself, we can determine the basic characteristics of its axial modes, which is the parts that we desire within our case and setup.

3.2.2 Cavity Geometry and Normal Modes

As the input light (the laser beam) is not an infinite planar wave, but is instead a gaussian waveform instead, the waveform will have other, normal modes that is also excited by the cavity structures as well. To look at what normal modes are excited by the cavity, we must look upon how the mirrors are characterized upon the cavity themselves. Due to that, the simplest method is to define the following two factors of the cavity:

$$g_1 = 1 - \frac{L}{R_1}, g_2 = 1 - \frac{L}{R_2} \tag{3.5}$$

Here, R_1 and R_2 are the focal lengths of the cavity mirrors. By utilizing these two factors, and the calculations of gaussian properties, we can get to calculations of crucial beam spot results:

$$z_1 = \frac{g_2(1-g_1)}{g_1+g_2-2g_1g_2}, z_2 = \frac{g_1(1-g_2)}{g_1+g_2-2g_1g_2} \tag{3.6}$$

Here, g_1, g_2 are the parameters specified in equation 3.5.

With the beam waist being given by:

$$w_0 = \frac{L\lambda}{\pi}\sqrt{\frac{g_1g_2(1-g_1g_2)}{(g_1+g_2-2g_1g_2)^2}} \tag{3.7}$$

Here, the g_1, g_2 are the same.

With the beam ends being calculated as

$$w_1 = \frac{L\lambda}{\pi}\sqrt{\frac{g_2}{g_1(1-g_1g_2)}}, w_2 = \frac{L\lambda}{\pi}\sqrt{\frac{g_2}{g_1(1-g_1g_2)}} \tag{3.8}$$

By utilizing these characteristics, we can utilize these information to view on how the gaussian waveform will act within the cavity. Additionally, these characteristics can also be used on characterizing and modeling the stability of the resonator and how it will react overall as well. [15]. With the various parameters illustrated and hidden above, we can also specify some range of parameters where the fabry perot will possess a stable solution. Using some algebra from the previous equations, the inequality is determined to be

$$0 \leq g_1g_2 \leq 1 \tag{3.9}$$

With the values of the stability of the resonator, we would be able to choose the extremas within this plot, which will correspond to a rather specific types of resonators that can react in different ways later on. The three types would be planar resonator, confocal resonators, and concentric resonators. One of the characteristics of the gaussian beam is that it has an additional phase shift attached to it known as Gouy Phase shift. The phase shift, which is an arctan function of varying widths, is also dependent on the transverse mode of the gaussian beam as well (which is represented by Hermite polynomials). Thanks to this additional phase shift, this would imply that the transverse mode of the gaussian beam would have a slightly different resonant frequency than the base beam, since it adds or subtracts a small amount of phase shift from the light itself. With the calculations we have made before and with lots of algebra, we can determine that the allowed resonances caused by this additional phase shifts can be written in the form of

$$\omega = [q + (n + m + 1)\frac{cos^{-1}(\pm\sqrt{g_1 g_2})}{\pi}] \times \frac{2\pi c}{2L} \tag{3.10}$$

Where q, m, n are integer multiples [15]. However, there is still a lot more to specify about the transverse modes than this though. The transverse mode will depend on the three extreme solutions we have witnessed previously, the confocal, planar, and concentric resonators will lean towards different trends. The confocal cavity would have its transverse modes be degenerate, the near planar scatters them to the right (higher), and with the near concentric cavities scattering the transverse mode frequencies to the left [15].

With the Hermite Gaussian modes being orthogonal with one another and the by having infinitely many modes as well, we have a space that can span to now, allowing us to create any image for an instant. However, due to frequency differences between the modes, this will not remain. This can be done through fourier analysis to select out and observe one of the modes and in a generalized resonance system

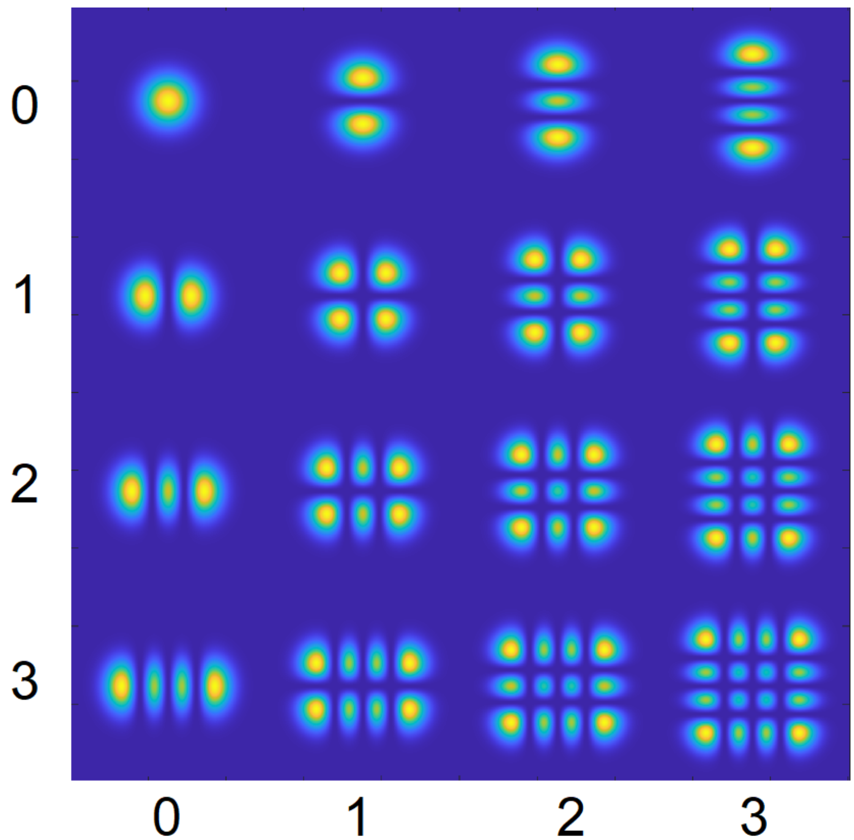

Figure 3.3: Intensity of the Hermite Gaussian Modes. Notice how the beam diameter increases as we get higher order mode. Generated from a MatLab Code with minor edits [16]

like this with wave equation solutions, we can represent an arbitrary wave equation as a sum of these modes, though this will mean that some methods of beam shape being entered into the cavity will be a very bad fit since it would not remain relatively steady and possess many peaks in which it resonates (and reduces the peak for the main peak we want). This is a bad thing since, except for a very specific exception, will yield many frequency peaks at different frequencies, making the system not work quite well as a frequency reference (especially given the fact that due to the finite window size of the cavity itself, larger modes will fall off quickly). What we want would be the mode of TEM-00 which is the base mode of Hermite-Gaussian mode and is depicted within 3.3 on its upper lefthand corner. Doing that will allow us to gain greater stability by allowing a specific mode to much brighter than others and minimize inter-mode beating that arises from adding all of these modes up together. So in order to overcome it, we must input the light exactly as how the mode we want, TEM-00, will resonate as. This can be done using our 3.7 and 3.8 that we have calculated previously. By beam shaping to the correct mode, we can suppress undesired mode as much as possible, thereby improving the performance of the locking mechanism. In order to find a way to do that, we can utilize a simple analysis through matrix calculations since it would keep account of beam size, and the rate of change for the beam size as well. By utilizing matrix and with our previous calculations of beam waist and the width of the gaussian beam at the ends, we will yield a matrix polynomial and, by numerical calculation, look for the necessary distance and focal length for the lenses to create the beam shape that we desire.

3.2.3 Power Enhancements

The power enhancement within the cavity can be found in similar ways as how we got calculations for reflectivity and transmission constants. Changing the thing out a little bit, we can see that given the reflectivity of the mirrors, the power enhancement within the fabry perot cavity is

$$\kappa = \frac{I_{inside}}{I_{input}} = \frac{Finesse}{\pi} \tag{3.11}$$

This pose as an important consideration to ensure that we don't accidentally burn off the internal mirror and will prove quite useful for later parts of the experiment as well.

3.3 Pound-Drever-Hall Lock

3.3.1 Basic mechanisms and signal processing

While the fabry perot serves as an excellent optical reference, we must try to lock it into reference to let our optical clock be as stable. To do that, we must electronically control the laser to mitigate the frequency noise of the laser, which is largely driven through current noise. However, this poses a problem since as shown earlier within the 3.1, one of the major challenges for the fabry perot is finding a way to lock into it. With the response being symmetric, we don't know whether we should increase or decrease the frequency in order to resonate properly, and in order to minimize frequency noises which will lead to line broadening, we would need a fast method to stabilize this as quickly as possible.

To do that, we would need to change this symmetric function into something asymmetric in order to know immediately which direction to choose in order to lock onto resonance. Furthermore, a region of linearity will also be a well wanted feature since that would allow us to implement a simple PID controller to get a quick control system to try and stabilize the laser.

For these many benefits, locking would be preferential and the first step to do that is to utilize a phase modulator to create side bands. Creating the side bands can

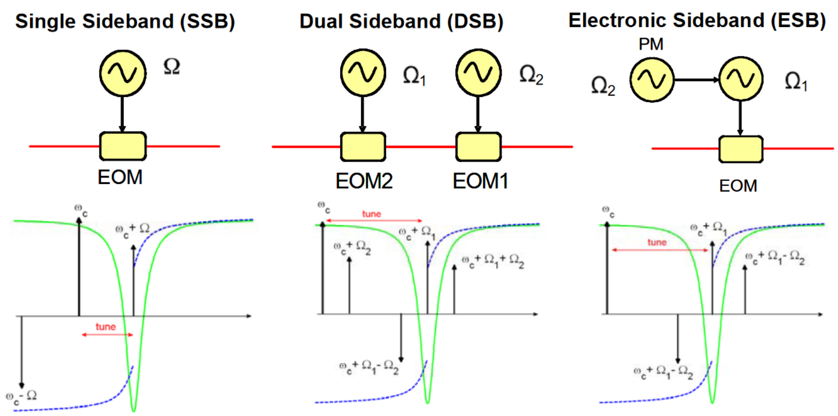

Figure 3.4: Illustrations of how different modulations of PDH signals work. As shown within the diagram, the electronic sideband would be the best since it would allow us to lock properly to the bottom of the fringe while minimizing unnecessary fringes that our light will be diverted to. Obtained with permission [17]

be done by simply modulating the phase of the light with a sine wave inside of it. Due to how narrow the cavity linewidth and the atomic linewidth will be, we need to introduce a level of tunability, to do that, the easiest method will be to introduce side bands to the original side bands to begin with, since that would allow us to maintain two different phases to add separate pairs of frequency to be modulated, we can allow one to be variable while leaving the other fixed. The machinations of this setup is illustrated in the figure 3.4:

By utilizing electrical modulated signal beforehand, we can reduce the total amount of spikes present within the setup, allowing us to have a more robust performance, since less light will be diverted to useless spikes.

The light is adjusted through an EOM which modulates the phase of the light with an electrical voltage input (an electronically phase modulated sine wave) which is then inputted into the fabry perot interferometer. From the fabry perot interferometer, we collect the reflected light and get into a photodetector, which is mixed with an oscillator frequency (the fixed one which is the innermost modulated one), which is then passed through a lowpass filter.

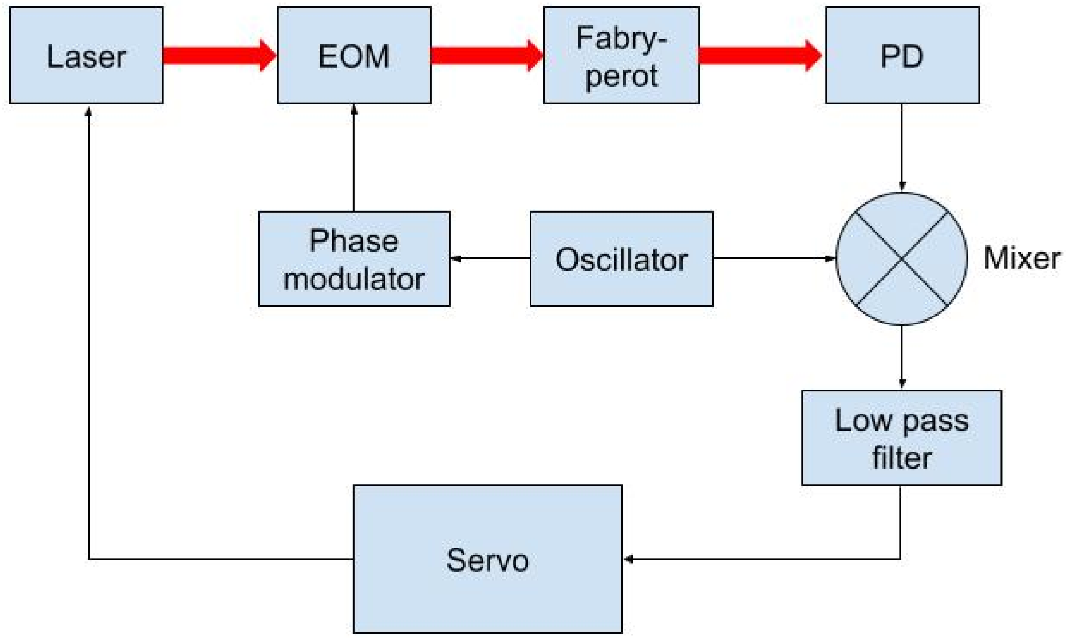

Figure 3.5: Illustration of Signal Processing of PDH

Method of electronic modulation gives us many benefits from other alternatives since this method allows us to create wide range scanning with ease and power efficiency in exchange for sacrificing some of signal. Another popular method is through AOM, which utilizes RF acoustics to diffract the light with frequency offset, while they are stable and allows for a moderately tunable range, with the amount we must go through (the entire FSR of the cavity), the AOMs would be a poor choice since it would yield a complex setup that is not only expensive, but power inefficient as well.

In order to counteract that, we can utilize the EOM to try to manipulate the sidebands to be tunable. If we were to just manipulate the sideband on their own, the locking performances would be poor as the only thing it can rely upon would be the singular sideband, and would slightly diverge from the standard PDH setup. Another alternative would be to apply the EOM phase modulation twice but that would create lots of redundant sidebands that would not help us with our tunable locking mechanism. So, the electrically modulated sidebands would be the best way in our case.

Let's do a quick rundown on the analysis of what happens to the reflected electric field, but due to the absolute amount of terms in this case, I'll gloss over the mathematical derivation for the most part. The electric field, which is now modulated to 7 different spikes, which is then multiplied to itself by measuring the power of the light (which is electric field squared). But with the mixing and the low pass filter combo, we can get rid of basically all of them and get a nice DC signal of the following form:

$$error = 2\sqrt{P_c P_s} Im[R(\Delta\omega)R^*(\Delta\omega + \Omega) - R^*(\Delta\omega)R(\Delta\omega - \Omega)] \tag{3.12}$$

for P_c and P_s being the ratio of the electrical modulation to the adjustable oscillator, with Ω being the fixed oscillation frequency. The R is the reflectivity of the cavity which is represented in equation 3.2 and R^* being the conjugate of that reflectivity. The $\Delta\omega$ is the frequency difference being a particular resonant mode and the light frequency. Therefore, the figure below depicts how the symmetric response of the fabry perot cavity now gets transformed into the asymmetric response of the PDH signal. Note the region of linearity in the middle, this would allow us to utilize the region for electronic control with ease since engineering linear control systems are very well developed. Now this would allow us to tune the laser through the entire FSR, allowing us to use the laser to be an optical clock wherever the frequency may be at.

3.3.2 Ideal Modulation and Noise Analysis

It is worthwhile to discuss the EOM for it works. The EOM works by using a material that changes its index of refraction by the electric field that is applied to it, and from the change in the index of refraction, the phase of the light passing through is now

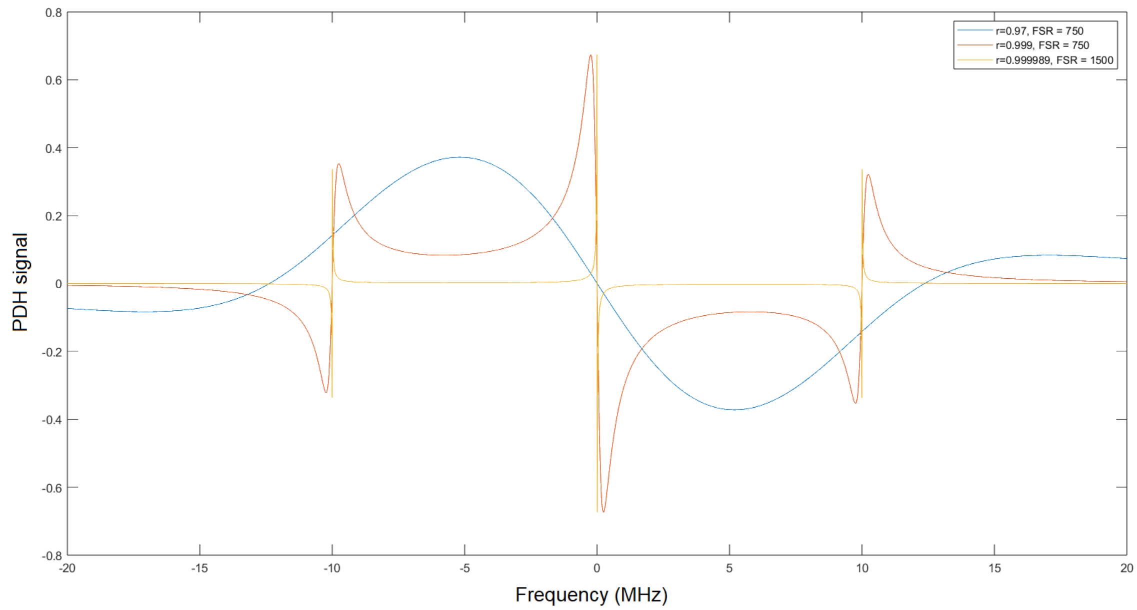

Figure 3.6: A PDH signal response with a $\omega = 10$ MHz, varying FSR and varying reflectivity. We see that the higher the reflectivity, the sharper the signal.

modulated, proportional to the voltage applied to the EOM to begin with. However, with the frequency modulation, the EOM delivers its results in the form of bessel function. The Bessel function is involved due to the phase shifting identity being deconstructed as this. Due to that, the maximum modulation depth of our signal itself must be at the maximum of J_1. Which will maximize the adjustable sidebands giving us the maximum signal to noise that we can with this setup. One of the most crucial aspects of measuring the noise figure in this system is the slope of the PDH linear region as this allows us to get better noise figures since it would allow us to get better feedback and faster feedback without utilizing outside sources which forces us to compromise in one way or another (additional noise introduced and making the system slower). While an indepth noise analysis is indeed possible, its process is not only tedious, but it is also not likely for us to get close to the shot noise limit within our system to begin with (other noise contributors will probably hurt us beforehand).

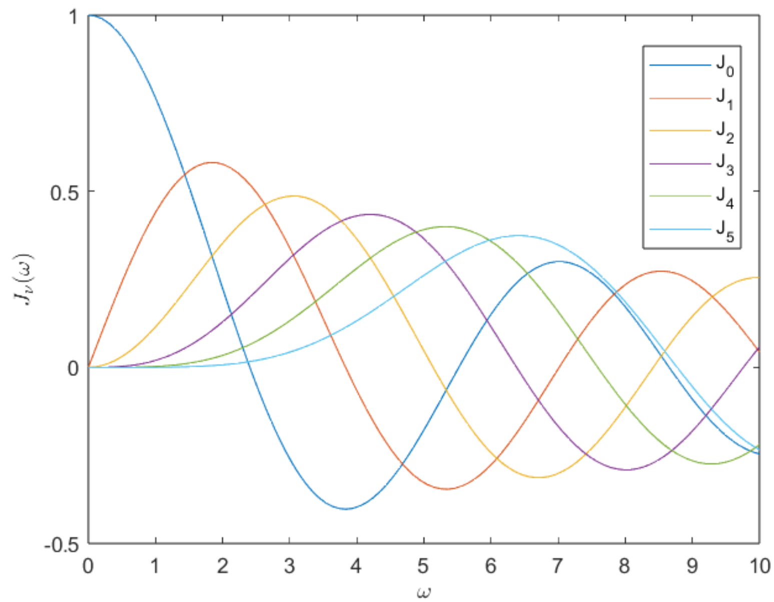

Figure 3.7: Bessel function of order J_ν

Regardless, further details can be seen within [18].

3.3.3 Fundamental shot noise analysis

Given how the control system has been setup, the fundamental noise boundaries we are placed in would be the length noise of the cavity and the shot noise of the photodetector. The length noise of the cavity shifts the frequency reference by the mirror separation changing over time, largely due to temperature. This has been averted in our situation by using a carefully engineered system to minimize that as much as possible. Furthermore, the medium within the cavity itself (the air) has been removed by the ultra low vacuum of the system as well.

The shot noise is caused by the discrete nature of the photons as it excites the electrons of the photodiode. To look upon it, we know that the light delivered are discrete, meaning that if we have an average power delivery of

$$\Phi = \frac{P}{h\nu} \tag{3.13}$$

Where $h\nu$ is the energy each individual photons, P is the power, and Φ is the mean photon count over a time period. Given from these, we can determine that with a realistic photodiode with a imperfect quantum efficiency, meaning that not all of the photons will emit and electron, we would get

$$\bar{N}_e = \eta \Phi \Delta t \tag{3.14}$$

Where η is the quantum efficiency, Δt is the time period, and $\bar{N}_e$ is the amount of average electrons we get over the time period. Since the electrons delivered would also be a poisson distribution, we know that the variance of photons would be $\bar{N}_e$ as well. Here, we can calculate the standard deviation by just taking the square root of the variance.

While currents in discrete natures may be difficult to conceptualize and define, by representing each of these arrivals as a simple impulse function would allow us to calculate the current. To do that, let us define $\bar{I}$ would be

$$\bar{I} = \frac{e}{T}\eta \bar{N}_e \tag{3.15}$$

Where $T = \frac{1}{2B}$ to be the resolution time of the photodetector itself. Additionally, its variance would be

$$\Delta I = (\frac{e}{T})^2 \eta \bar{N}_e = 2eIB \tag{3.16}$$

Where e is the charge of electron, I is the current output of the photodiode, and B is the bandwidth of the photodiode. To get a better description over its derivations, please check *Fundamentals of Photonics* [12].

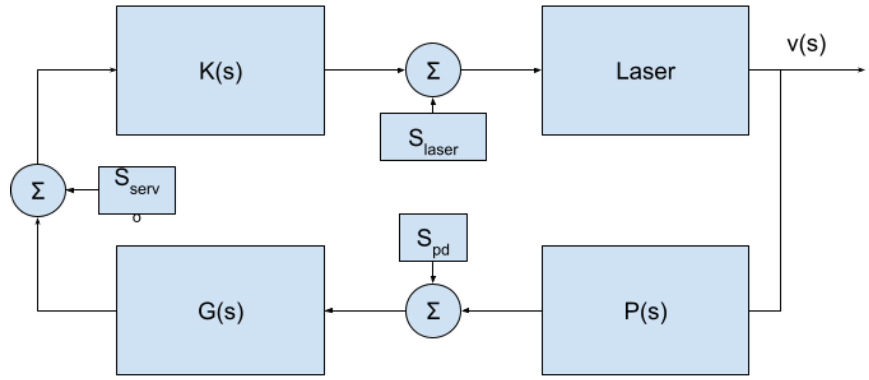

Figure 3.8: Control loop of the pound drever hall system, K here is the gain of the laser actuator (Hz/V), P here refers to the Pound Drever Hall Gain (V/Hz), and G here refers to the servo gain to the system (V/V). These are all linear contributors to noise; however, since pound drever hall is a nonlinear signal processing method, the noise for the photodetector and cavity noise has been combined to a singular noise.

A pound-drever-hall system and its noises can be modeled as a simple control loop like in figure 3.8

Using simple independent, linear noise in a closed loop analysis, the transfer function for the noise that we obtain is:

$$S_{tot} = \frac{S_{laser} + KS_{servo} + KGS_{pd}}{1 + GPK} \tag{3.17}$$

While P is a nonlinear response, around resonance, we can approximate P as the linear slope that we have mentioned earlier. Furthermore, the noise S_{pd} is combining both the photodetector noise which will be added before the mixing and the cavity noise, which will impart the cavity as well. Due to their nonlinear nature, complex analysis will be refrained, but there are two things to know from here: firstly, the calculation for the length noise will be rather difficult unless a small-change approximation is made, and secondly, the noise from the photodetector and the discriminator circuit is tacked on, allowing us to analyze it at a greater ease than the first. Since the cavity is designed for minimal noise, we know that the leading noise will not be from the cavity, but would be from the electronics instead. This method will be frequently used to get a sense of how much linewidth narrowing we can do in a given system frequently, since both are rather easy to measure. However, this will not tell us what the fundamental noise level we can reach down to is; to do that, we must approach it in a different way. However, by increasing the gain of the servo to a very high level, we can actually approximate the noise as the following equation: [17]

$$S_{tot} = \frac{S_{pd}}{P} \approx \frac{S_{pd}}{D_\nu} \tag{3.18}$$

So we must also calculate the slope of the pdh as well (V/Hz). To get the slope, we will go back to the equation 3.2, where if we were to model the input frequency as a small perturbation away from resonance ($\omega \approx N * FSR + \delta f$), we would get equation 3.19 by utilizing small angle approximation.

$$F(\omega) \approx \frac{r}{1-r^2}(i\frac{\delta f}{FSR}) = \frac{iF\delta f}{FSR} \tag{3.19}$$

By carrier frequency being near the resonance and the side bands being very far from the carrier frequency, we can approximate the photodetector response as the following equation:

$$P \approx 2P_s - 4\sqrt{P_c P_s} Im[F(\omega)] sin(\Omega t) + 2\Omega \approx 2P_s - 4\sqrt{P_c P_s}\frac{F\delta f}{FSR} + 2\Omega \tag{3.20}$$

So using 3.20, we would get the error signal of

$$error = -4\sqrt{P_c P_s}\frac{F}{FSR}\delta f \tag{3.21}$$

Giving us the slope of

$$D = 4\sqrt{P_c P_s}\frac{F}{FSR} \tag{3.22}$$

Where F is the finesse of the cavity [17]. This would give us the slope of (W/Hz), to utilize it for measurement in our case, we would have to convert it to V/Hz. So we would have to characterize the photodetector to change the slope from power to voltage.

Chapter 4

Implementation

To implement the Pound Drever Locking mechanism to our laser, we would have two elements to dominate its performance: a photodetector and a cavity. While these two are the most important parts of the locking and what most of the discussion will be spent on, other parts could be introduced quickly here as well.

Since the ultra high finesse cavity is not confocal, we would have to add mode matching lenses to mode match into a single mode, which would be TEM-00 in our case. In order for that to happen, we must change our collimated laser beam into the beam diameter and the beam angle of a resonating TEM-00 in our cavity. After calculations, we found out that a pair of lenses with focal lengths, 100 mm for the first lens and -50 mm for the second lens, worked with distance separation of 3.6 cm away from each other, and with the second lens 20.3 cm away from the planer mirror of the cavity.

Furthermore, since our performance heavily depends on how much reflected light we can get back, we must maximize our reflected light to improve our performance. To do that, we would incorporate two optical components: a polarizing beam splitter and a quarter wave plate. The polarizing beam splitter will let lights of specific angle of linear polarization pass through, and lights of perpendicular linear polarizing to

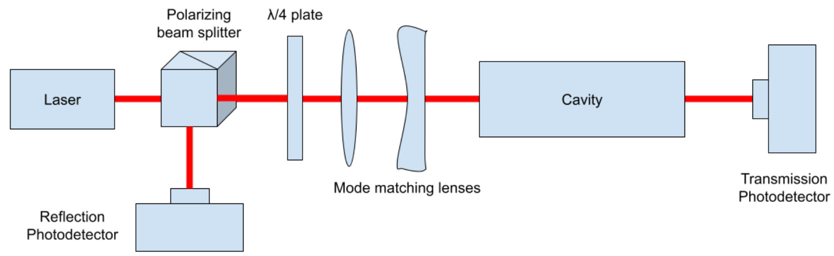

Figure 4.1: The light, which is a collimated monochromatic light, will go through the polarizing beam splitter, quarter wave plate, mode matching lenses, then the cavity to be reflected off and go through the entire chain backwards where it gets reflected by the polarizing beam splitter to go to the photodetector. The transmission light just goes through it all.

reflect. A quarter wave plate will turn a linearly polarized light into circularly polarized light and vice versa. Since our laser light is a linearly polarized, gaussian beam output, we can firstly let it pass through the beam splitter without any reflections. Afterwards, the quarter wave plate will turn the linearly polarized light into circularly polarized light, where it goes through the mode matching lenses and reflect off of the cavity (we only care about our reflection in this case). The reflected light will now have its phase flipped, meaning that the polarization will flip its sign. As we go back through the quarter wave plate once more, the circularly polarized light of flipped sign will now become a linear light that has been rotated by $\pi/2$, this will now reflect entirely off of the polarizing beam splitter, sending all of the reflection to the photodetector. This optical setup would allow us to maximize our signals in the ultra high finesse cavity as shown in figure 4.1. However, for the 97 percent and 99.9 percent cavity, we forego mode matching as the cavity is confocal and rather than using a polarizing beam splitter and a quarter wave plate, we have used a normal 50/50 beam splitter. This would only allow one fourth of the incoming light to be sent to the polarizing beam splitter, making our performance worse there.

4.1 Photodetector

The photodetector circuit utilizes a photocurrent and runs it through a transimpedance amplifier to change light into voltage signals 4.2 Since the PDH signal involves a mixing step of approximately the carrier frequency, the photodetector circuit must have a high bandwidth to let the RF frequency of the carrier frequency through. However, due to the photodiodes possessing their own capacitance, we would be limited by how much resistance we can add for the voltage gain before the RC time constant becomes too large. So, one thing that we can do to counteract that is to utilize a small resistor to reduce the RC constant while using a secondary step of amplification to get more voltage gain; however, this will make the signal susceptible to two stages of noise instead. By adding these two setups, we have measured the noise of the amplifier setup to yield a noise of 750 μV of noise. Within the specification of the photodiode itself (FT-100), the typical photodiode utilized for this setup would give us a noise of approximately 14.4 μV of noise, meaning that the majority of the noise that comes from our setup arises from the amplifier circuit we have set up.

However, as mentioned earlier, the photodiode has its own engrained noise added onto it. The noise of the photodiode would be dependent on shot noise as well.

The measurement for our light is 0.4 mW input for the Thorlabs Photodiode PD10A, from there, we can calculate that the shot noise within our system will be 8.9 mV. Our own DIY made photodetector circuit powered by a photodiode would have the shot noise level of $6.4 \times 10^{-4} V$ by using the measured values of 0.8 mW of incoming light, resistor gain of 4800 Ω, and the properties of photodiode and used the equation 3.16 and our photodetector setup.

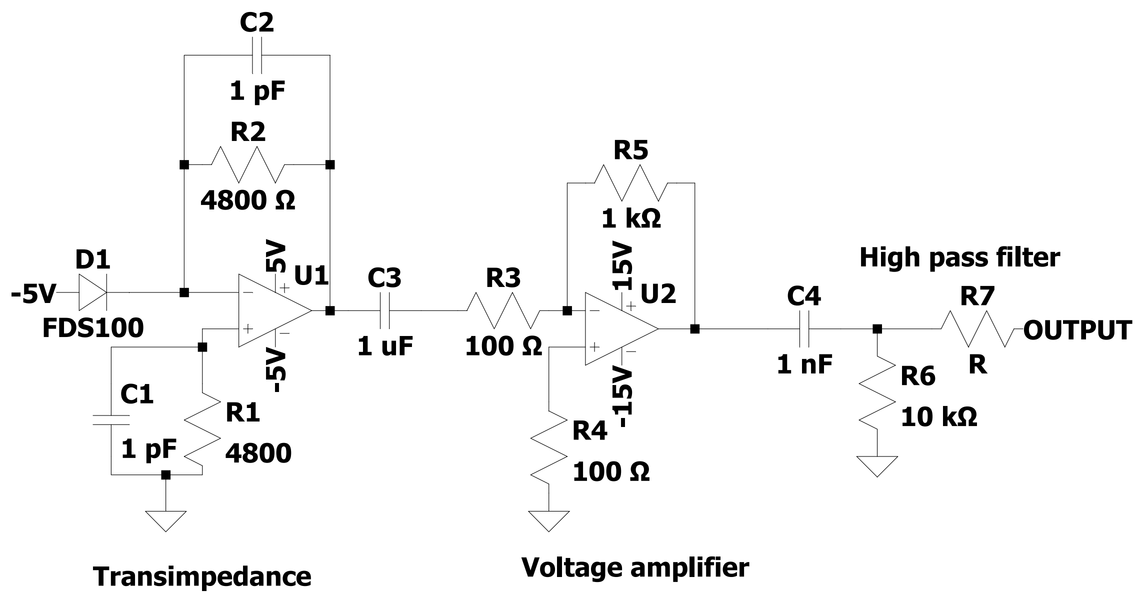

Figure 4.2: The photodetector utilizes a photodiode, biased with a negative voltage, which will draw current as light shines upon it. That current gets put into a transimpedance amplifier with a gain of 4800 Ω. The DC response will then be cut off, afterwards the signal then get fed into a voltage amplifier with a gain of 10. That signal is then sent on a highpass filter with a 50 Ω resistor for impedance matching.

4.2 Linewidth Measurement

While we could measure the linewidth optically either by obtaining a same laser as indicated in source, or by getting a large amount of fiber optic and an AOM and measuring the beat frequency power spectral density, but, due to budget and time constraint, we were not able to do it for now. Nevertheless, we can approximate the current frequency of the laser by looking into the Pound Drever Hall signal, and this will serve as a nice preliminary measurement to help us gauge our performance roughly. For example, the conventional method of self-heterodyning the laser signal with a fiber and an AOM would not work in our case since that would require us to gain enough fiber to surpass the laser's coherence length. The target linewidth is 100 Hz, if we were to use that value and a conventional fiber to calculate the coherence length, we would a length greater than 10^6 m of fiber. Since fibers attenuate by a significant amount, we would be attenuated to nothing over that period of length. The secondary option for measurement would have been to prepare an identical setup of laser to heterodyne with one another. However, that would require us to prepare two of these laser setups which would be uneconomical and time consuming. The last object for consideration would have been to do a self-heterodyne measurement without extending it past the coherence length. There are numerous papers, which state that through careful modeling and careful analysis of PSD, approximations of linewidth is indeed possible [19]; this would have been the most feasible within the lab, but due to time constraints, I was not able to do it unfortunately.

To assess the linewidth of the laser broadened by the frequency jittering around, we can model the linewidth by the following formula which was derived from modeling the laser linewidth broadening caused by white noise.

$$\delta f = \sqrt{8 \ln(2) A} \tag{4.1}$$

Where δf refers to the linewidth of the laser and A refers to the area under the curve when the power spectral density satisfies the following inequality:

$$P(f) \geq \frac{8 \ln(2)}{\pi^2} f \tag{4.2}$$

Where $P(f)$ is the PSD value of the laser at that point and f being the frequency noise frequency. [20] [21]

The integration of noise only occurring in represents the linewidth being much more sensitive to broadening on lower frequencies, with the higher frequencies making it more prone to "wing-ing" as termed in the article, which refers to the creation of the sideband due to frequency modulation. This makes it so that lower frequency jitters will affect the linewidth more the phase modulation these types of noise cause will occur much closer to the carrier frequency, which will make impacting that carrier frequency far more easier.

4.3 97-percent Fabry Perot Cavity

Going off from the cavity theory we have mentioned earlier, the cavity can now be characterized and it is as follows: the reflectivity of the mirror r = 0.97. The mirrors are separated with distance of 300 mm, with the focal lengths of the mirrors being 300 mm as well. This would give us the parameters of $g_1 = 1, g_2 = 1$ each. Furthermore, we are inputting 1.2 mW of light while using a 50/50 beam splitter, potentially bringing us 0.3 mW of light into the photodetector. If mode matched perfectly, all of it should resonate; however, but by utilizing an imperfectly collimated beam, we will not get a complete resonance, meaning us locking to these cavities (97 percent and 99.9 percent cavities) will not be close to its maximum performance.

4.3.1 Standard Pound-Drever Hall Lock

To measure the slope of the Pound drever hall within our setup, we have just scanned the frequency of the laser and converted the time separation into a frequency separation instead. From that, we have determined that the slope of the laser with a single side band of Pound Drever Hall signal would be 1.509×10^{-8} V/Hz as indicated within figure 4.3.

With the measurement of the slope, and the measurement of the noise of the photodetector, we can estimate the yielding noise from the light input which gives us the shot noise and the slope netting us with a linewidth of 587 kHz as our best possible linewidth for this system. However, this is likely inaccurate since the assumption of all of the light being reflected from the fabry perot will be resonant is a faulty one. If we were to utilize what the photodetector actually measures, then we would get a linewidth measurement of 200 kHz.

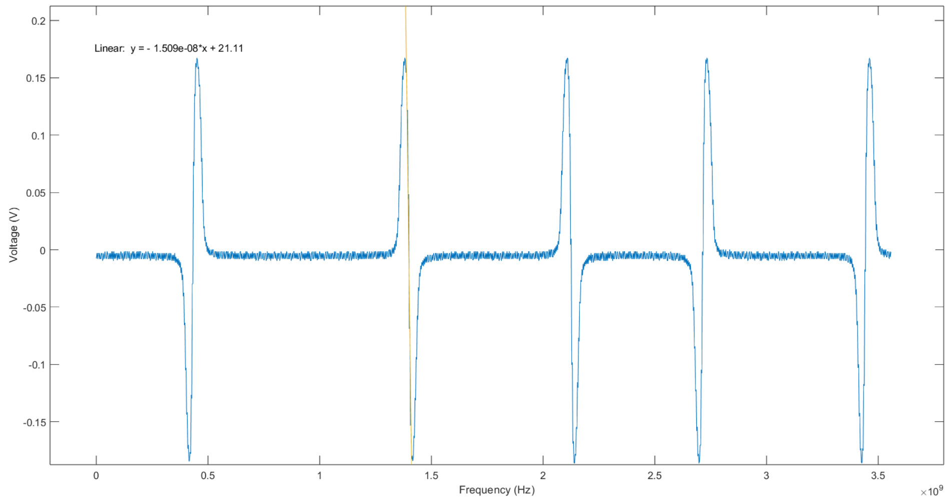

Figure 4.3: The pound drever hall signal of 97 percent cavity with its slope fitted in as well. The signal repeats in this case, since we are tuning more than one FSR with the laser. The reason for that is to check the FSR of the cavity, convert it to the constant voltage slope of the ramping frequency, then convert the horizontal axis to frequency. Beyond a certain point, the signal flips due to the frequency ramping in the opposite direction.

To analyze the performance of the locking mechanism at a rough glance as well, we can utilize an allan deviation of the noise signal as well. The allan deviation is obtained by splicing the sample into M-samples then measuring variance present within. This method will allow us to measure the phase noise of the signal thereby giving us the estimate for how stable our clock would be.

As indicated in figure 4.4, we can see that the noise of the photodetector is a factor of ten smaller than the noise of the system itself; thereby suggesting that the written noise here would not be too significant. Additionally, the lack of attenuation in allan deviance with short samples show that the system is poor at addressing fast noise; however, that is less impactful since higher frequency noise contribute less to broadening than low frequency noise as indicated by the inequality referred in equation 4.2.

To get the measurement of the linewidth, we had to obtain the Power spectral

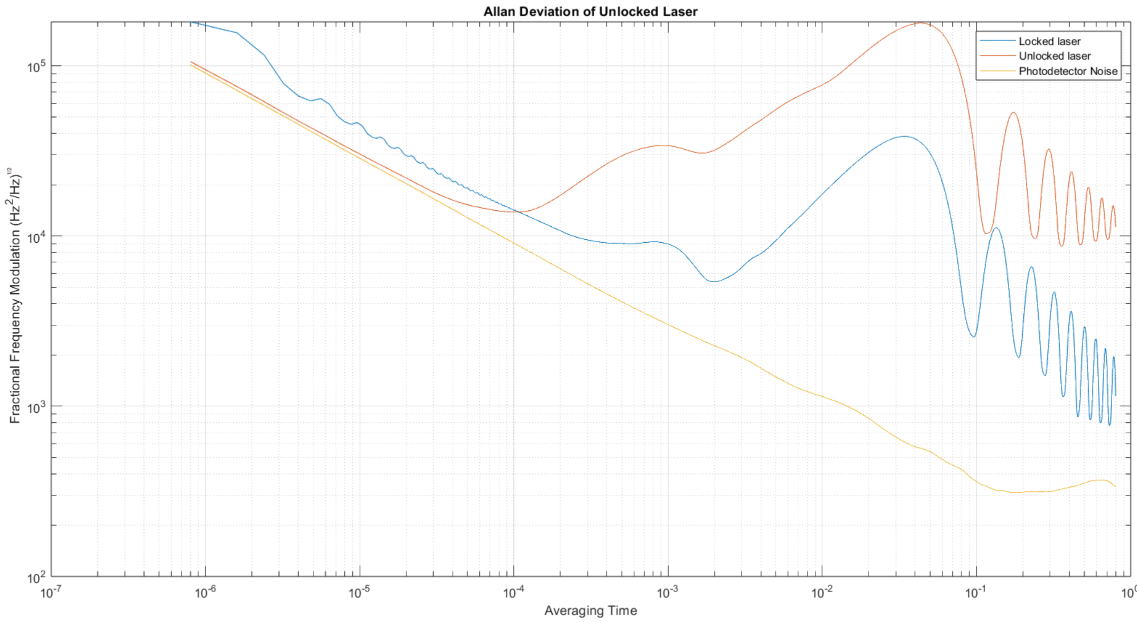

Figure 4.4: The allan deviation of the locked signal, the unlocked signal, and the photodetector. It shows the noise contribution of each and how locking reduces the noise of the signal. The presence of peaks in the locked signal implies that the signal is not locked on completely, but that is okay since this is just a demonstration beforehand.

density of laser frequency over time. Since the laser stayed within the linear regime of the pound drever hall, by analyzing the electronic response, we can "convert" it to laser frequency response (this is not foolproof as mentioned earlier, this will not account for actual electronic noise). So we have gathered the locked signal over long periods of time (10s), then converted the voltage into frequency, which we then used MatLab to approximate the power spectral density of the frequency over time.

With the approximated signal, we can extract where the signal goes above the inequality specified in equation 4.2, and integrate utilizing trapezoidal integral calculation.

The calculation of the integral and by putting it into equation 4.1, we get that the linewidth of the laser is approximately for 300 kHz the locked laser, from figure 4.5, and for 450 kHz the unlocked laser, from figure 4.6. This may show that the locking

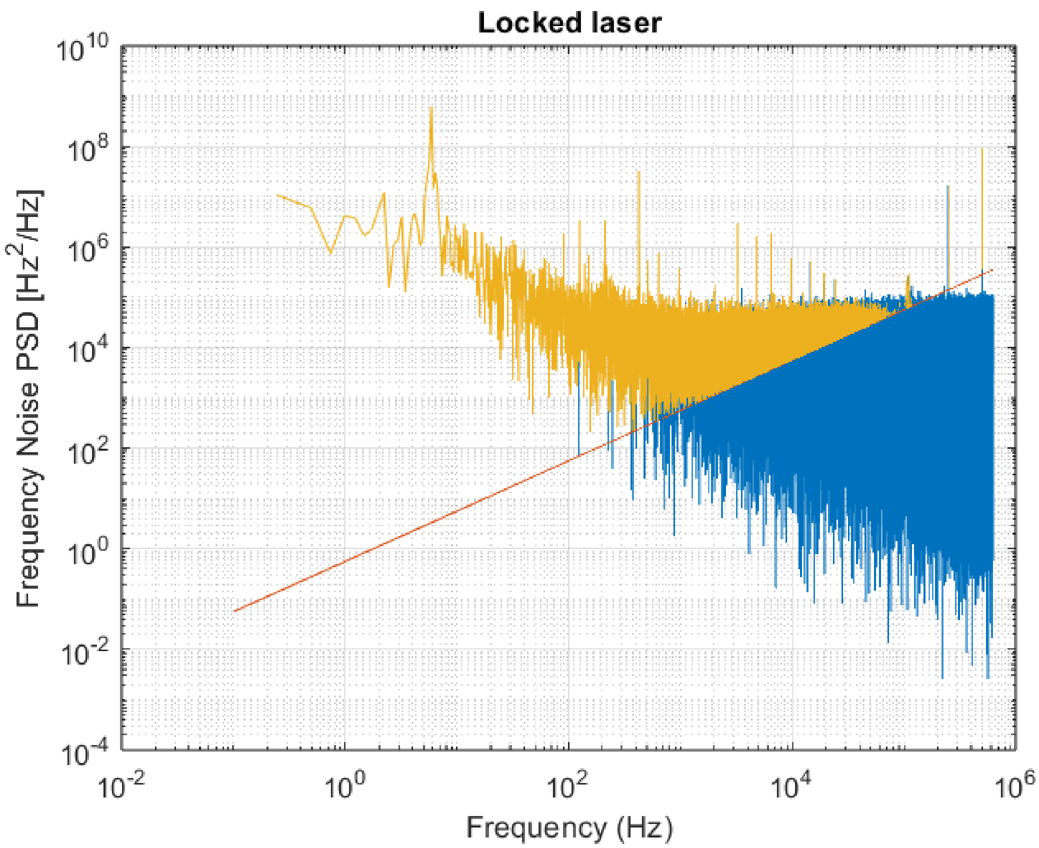

Figure 4.5: Power spectral density of the pound drever hall signal with the slope needed for the integration.

would currently perform worse than the laser's own tuning itself (which should be around 200 kHz), which would imply that we are now writing the noise of the system to the laser instead. However, with that, we now know that the current setup would be bad for trying to reach our target goal of down to 100 Hz.

Since the standard pound drever hall cavity performed subpar already, we should anticipate that the noise figure in the side band locking should perform 5.6 times worse than the method described here [18]. Thereby making it impossible to lock down to this particular cavity with the precision that we would need.

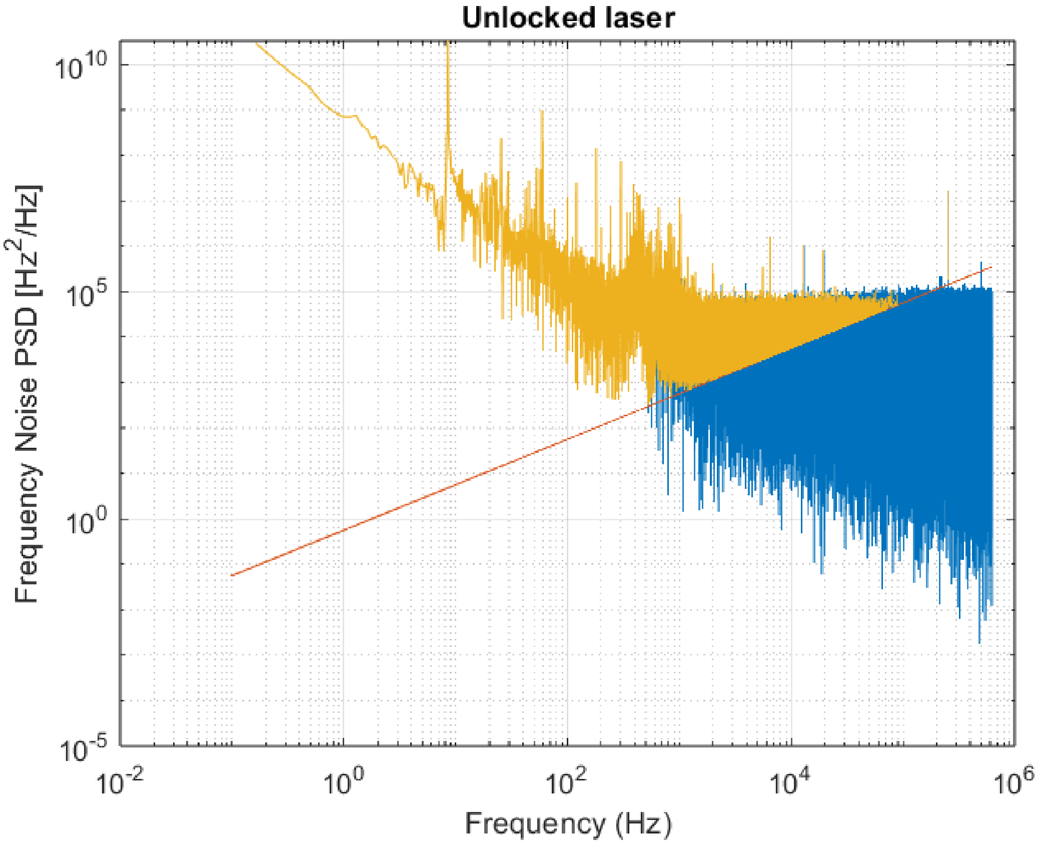

Figure 4.6: Power Spectral Density of the unlocked signal. Shows the signal being far more vulnerable to drift than the locked signal.

4.3.2 Tunable Electronic Locking

The tuneable electronic locking would incorporate a phase modulated signal into the EOM, giving us tunability and allows us to lock the laser offset to the cavity with a specific frequency (the microwave frequency). While we may get a worse performance overall, it would still be an interesting avenue to double check the performance loss of the locking signal as well. So, before anything, we have analyzed the slope of the pound drever hall once more. Using the same methods as described earlier, we have extracted the slope of the PDH signal by ramping the frequency of the laser as shown in 4.7.

This led us with a slope measurement of 1.983×10^{-9} V/Hz, giving us the theo-

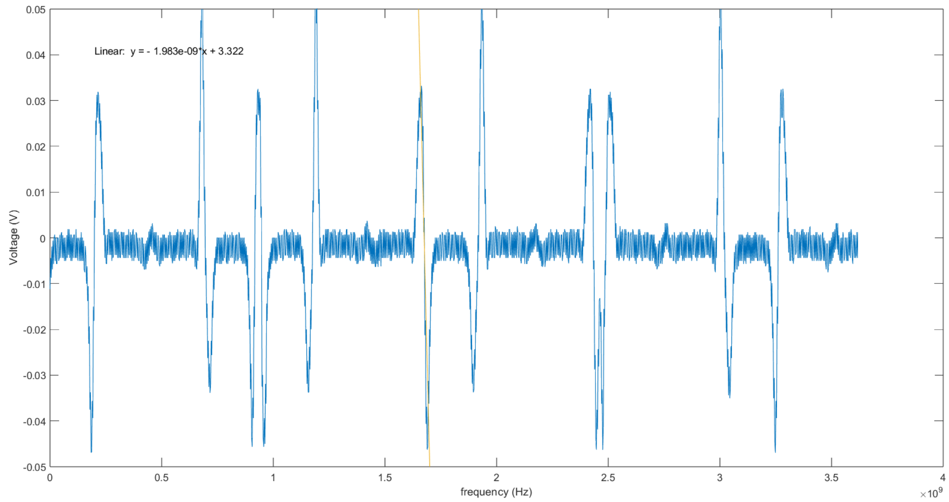

Figure 4.7: Shows the PDH signal of the sideband tuning. The signals are repeated here once more since we are ramping the laser beyond the FSR of the cavity, but this is a lot more messy as the side bands created by the electronic sidebands will also generate its own PDH signal. Because of that, we can see some of the PDH going in the opposite direction as the rest of the PDH signals (we can see a pattern of up, down, up (ramp up), then with down, up, down (ramp down).

retical best value of 4.5 MHz, but if we were to use a measured data, we would get 1.2 MHz instead. This is approximately 6 times worse than the value calculated from the pound drever hall before the electronic sideband. Showing us that while we are relatively close to ideal modulation, we are not quite there yet. Further adjustments could have made this better, but are not done due to time constraints.

Similar as before, we are also adding an allan deviation plot to characterize the noise of this lock as well. As shown in figure 4.8, it shows that our performance is now worse across the board when compared to the non-sideband locking in figure 4.4, as we have expected.

Now, we can go on to calculate the linewidth of our locked laser but looking at the power spectral density as before. As viewed in 4.9, we can see that the integration through the highlighted region, then fitting it into 4.1 will give us the value of the estimated linewidth.

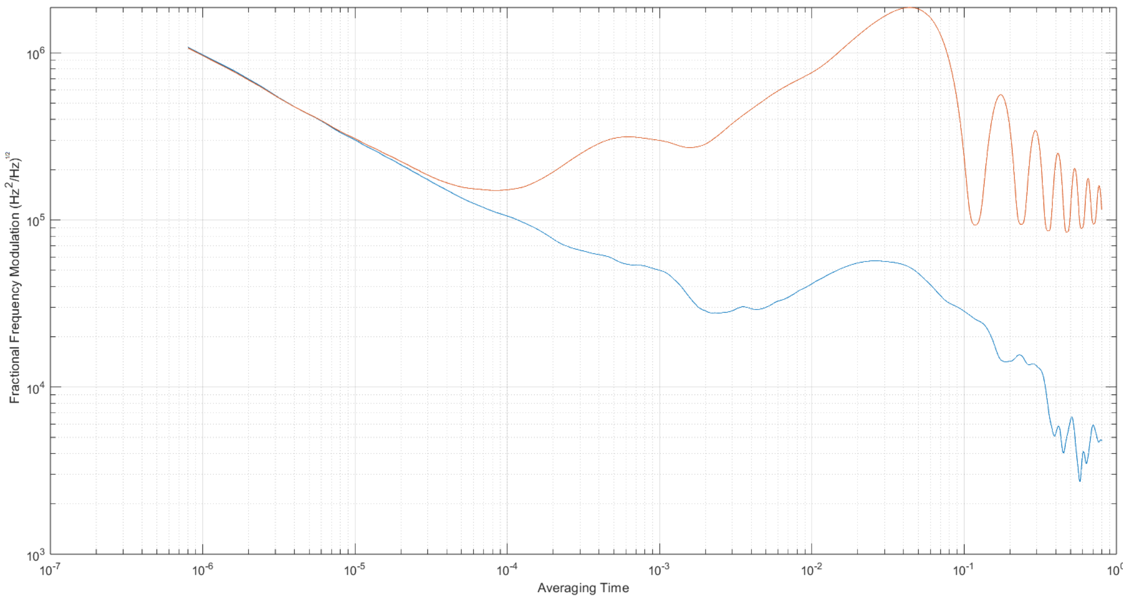

Figure 4.8: Shows the allan deviation between the unlocked and the locked signals, the unlocked signal has notably higher low frequency drift than the locked one.

Calculating from here, we will now get a linewidth of 2.6 MHz. This shows that our performance is now 8.7 times worse, showing to us that the system is not well attuned since the expected value should be around 5.6 instead.

By practicing with a cavity with a much smaller finesse, we can now raise it up to our intended finesse now.

4.4 Higher Finesse Setup

The ultra-high finesse cavity possesses a pair of mirrors that will reflect 99.9, yielding us a finesse of 1570. The higher finesse cavity will allow us to obtain a much higher voltage to frequency slope, allowing us to reduce the linewidth even further. However, as we would necessitate a single-laser spectroscopy, we would need to find a way to scan across continuously. While the pound drever hall signal to lock on at a singular location, we can lock at an alternative frequency by offsetting the lock point with an electronic sideband. As mentioned earlier, the Fabry-perot cavity possesses various

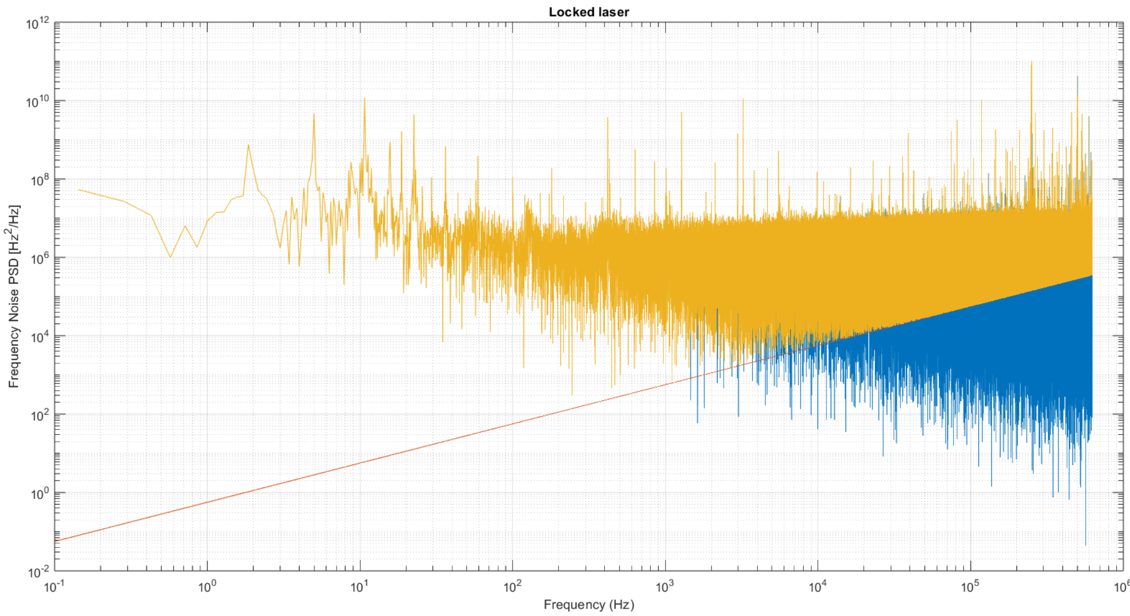

Figure 4.9: Shows the Power spectral density of the sideband locked laser, as expected, the laser now has a worse performance than the main lock.

sorts of axial modes, utilizing equation 3.1, we know that the FSR of the cavity will be 1.49896 GHz. That would mean that in order to run a fairly continuous spectroscopy, we would need a way to tune up to the range of at least 1.5 GHz. To do that, we have utilized a signal generator (Agilent 4433B) that will output a microwave frequency from 2.4 GHz to 4 GHz which is also frequency modulated with an 10 Mhz signal instead. Using fourier analysis, we can show that a frequency modulation of a single sine wave would be equivalent to a phase modulated signal with the same frequency. So, this microwave frequency will now allow us to offset the lock point, which can be controlled externally through a computer instead; thereby allowing us to lock our laser across the FSR, allowing us to do a spectroscopy with it. Given the radii for the focal points of the two lenses and the length separate of the mirrors will tell us that the two parameters to characterize the fabry perot cavity will be $g_1 = 0.8, g_2 = 1$ with each g's corresponding to the 500 mm and planar mirrors respectively. So as referenced earlier within the section regarding the degeneracy of the axial modes, this would not net us a degenerate setup as before and would require us to mode match into the cavity to maximize our signal being delivered to a singular mode. With the data, however, we will progress down the same path as well. The pound drever hall is created by using the EOM to create a tuneable electronic sideband, then utilizing the signal generator, we can lock onto the sideband frequency, which will allow us to tune across the entire FSR. However, due to the incredibly high finesse of the cavity, locking onto cavity did not proceed immediately. Before achieving that, we had to undergo an intermediary locking step with the 99.9 percent reflective cavity (or a cavity with the finesse of 1570) to properly characterize the new fabry-perot first. The slope of the signal would have been 2.94×10^{-3} V/Hz from the measurements of its incoming power of 0.8 mW, its modulation being at $\beta_1 = 1.84$ and $\beta_2 = 1.01$, the cavity finesse, and the photodetector properties. This would have led us with a best case scenario linewidth going down all the way down to 0.22 Hz, meaning that it is technically possible to go down to subhertz linewidths, barring other noises or factors preventing us. However, with non-ideal cable placements and with many sources of noise that may be added, we would most definitely not get to this level.

4.4.1 Locking onto the intermediary cavity

Locking onto the intermediary cavity was also not easy as the laser noise was greater than the cavity's normal parameters. So, we had to undergo a process of locking onto an intermediary cavity to get a better stability beforehand. To do that, we have utilized a 99.9 percent cavity to lock onto.

The slope of the 99.9 percent cavity at that point was approximately 1.5×10^{-6} V/Hz which is approximately 100 times better than the result found in 4.3. This should theoretically give us a 100 times better performance in narrowing linewidths, allowing us to get down to the linewidths of up to 6 kHz using the calculated value and 1.5 kHz if we were to utilize the measured value.

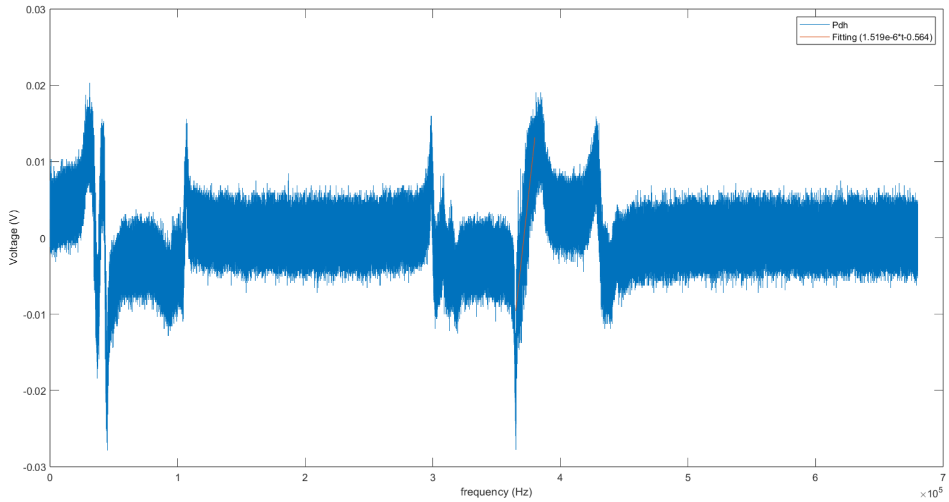

Figure 4.10: The Pound drever hall depicted here is significantly noisier than the one depicted in 97 percent pound drever hall since the laser is now more unstable than the cavity itself. Locking onto here should allow us to narrow the linewidth of the laser further.

With the much higher slope that we are receiving, we can now observe the allan deviation for the stability of our optical clock as well. When we look into its allan deviation in figure 4.11, we can observe that it is better than the 97 percent cavity by almost a factor of 100. This hints at the fact that our optical clock while locked to this cavity is significantly better than before.

By finding out the slope of the pound-drever hall itself, we can look into the PSD of the noise of the voltage signal of the locked laser as shown in figure 4.12, we can determine that the noise linewidth of the laser is now 2.2 kHz. This now shows that the laser linewidth is far below the level of 200 kHz of the laser itself. Although it is very well possible that we are writing electrical noise into the laser itself, we would be unable to measure it here with the measurement techniques utilized here.

With the laser now pre-stabilized, we can now try and observe the pound drever hall of the ultra high finesse cavity itself. By locking onto the cavity of 99.9 percent cavity then tuning it with a piezo, we can try and observe the ultra-high finesse cavity

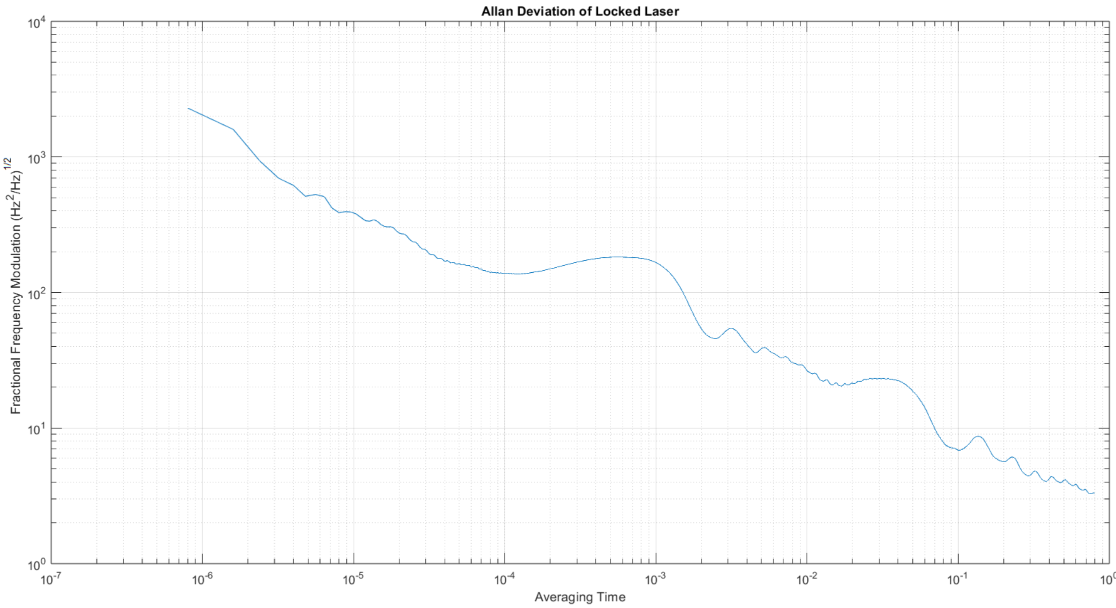

Figure 4.11: The Pound drever hall depicted here, which came from the 99.9 percent cavity, is significantly noisier than the one depicted in 97 percent pound drever hall since the laser is now more unstable than the cavity itself. Locking onto here should allow us to narrow the linewidth of the laser further.

without much trouble this time. However, due to my rapid time constraint, I was not able to progress much further than this, and must continue to the following sections with just the data I have procured for now.

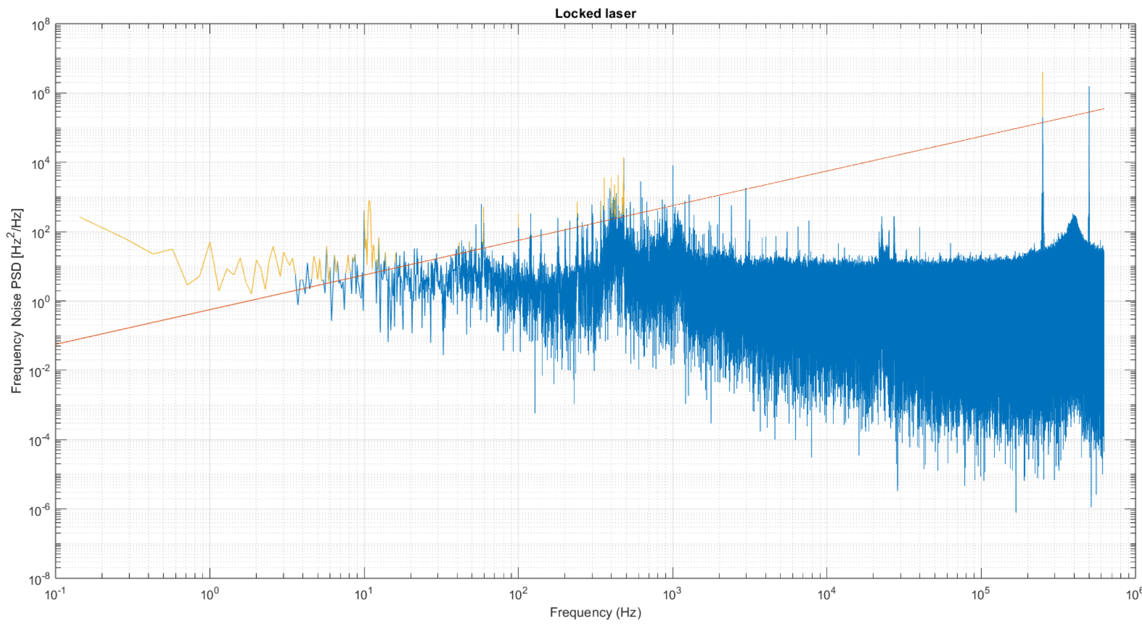

Figure 4.12: The Power spectral density of the laser frequency measurement, with the same inequality (equation 4.2) being used to determine the linewidth once more.

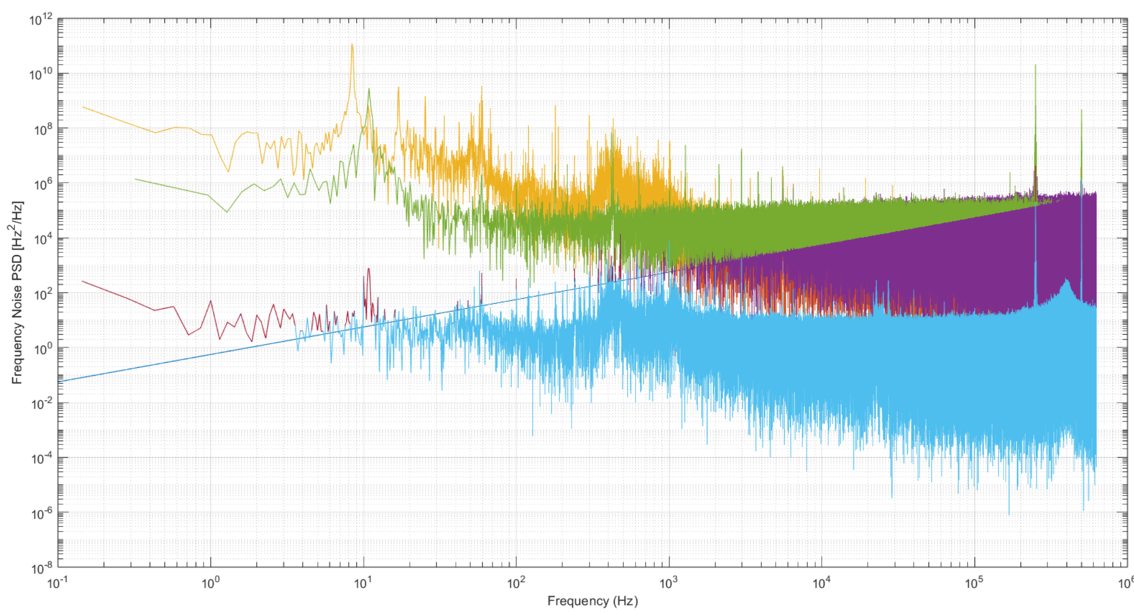

Figure 4.13: The upmost PSD curve is the unlocked laser, the middle is the one locked to 97 percent, the bottom one is locked to 99.9 percent cavity. While the lock to 97 percent hardly did anything (as expected), the lock onto 99.9 percent changed the PSD of the frequency noise quite significantly.

Chapter 5

Conclusion

There are many things that are left to be desired. For example, we were not able to lock onto the ultra high finesse cavity as the laser's jittering was too much for the locking mechanism to handle. While the feedback did try to hold onto it, the laser's frequency jitter made it impossible to stick around it for too long. What may be done to help with this is to undergo an intermediate laser stabilization to try and get the jitter down to a point where we can get the laser stable enough to try and get it stabilized to the ultra high finesse cavity. While we did manage to stabilize down to the 99.9 percent cavity to try and stabilize the laser down nearly one-hundredfold of its linewidth, perhaps jumping all the way down to without an intermediary step may have been a stretch. Given what we were able to stabilize down towards, with a linewidth of 2.2 kHz, this would allow us to get a measurement of μ with the uncertainty of $\frac{\Delta\mu}{\mu} = 6.8 \times 10^{-12}$, based on the calculations of 1.2 and previous calculations [22]. This poses too much immediate uncertainty to try and utilize it for long time scales. I would definitely have to try and get better linewidths than this before continuing. The next plan is to try and finish up the initial goal of locking the laser to the ultra-high finesse cavity. Currently, the laser appears to jitter around too profusely, forcing us to not be able to lock onto the super narrow dip in reflection of the ultra-high finesse cavity yet. Due to that, we were trying to look into an intermediary step to observe the cavity at the very least. However, due to the lack of time and preparation for going around that, we were not able to accomplish that, yet. The following plan would be to try and setup the plan for an intermediary cavity and a secondary PDH to try and setup a permanent intermediary lock, rather than using a Fabry Perot that is used elsewhere. Furthermore, for the tunable, electronic sideband, while it works, the ability to tune it is surprisingly finicky. With the lock only managing to hold with it by using the using the signal generator's own built-in scan function, we would have to explore the possibilities to integrate that into our system instead. While the code is incomplete at the moment, I do not anticipate it to be a particularly difficult process since most of it (talking with the signal generator, a simple space state machine for manually setting the frequency) is already setup and ready to go. While the measurement we used will serve as an adequate preliminary check, it is not the best way for measuring linewidth. The measurement that we are using is not accounting for the fact that the noise may be coming from elsewhere (electronic noises) and may actually be writing electronic noise into the laser instead, which would broaden the laser, not narrow it. With the electronic method of measurement, we are not able to consider for that. If we had more time, we would have tried alternative methods for linewidth measurement such as by measuring the linewidth by trying to get the model the short-delay self-heterodyne result instead or by utilizing the oxygen ion as our reference to instead. This is probably a good idea, since there are multiple evidences pointing towards the fact that some electrical noises are being written to the laser, which is increasing the linewidth instead. The steps that must be done to prepare ourselves for the upcoming measurement is to firstly increase the intensity of the light. This will be done in a two-step process where we will be using a tapered amplifier to do the first step. A tapered amplifier is a semiconductor which we will buy to implement this.

However, while tapered amplifiers will amplify the seed laser, or the input laser, it would also unfortunately output some spontaneously emitted photons due to vacuum fluctuations. However, by using a fabry perot cavity after this, we can remove most of them as we would now constrain ourselves geometrically once more to properly resonate. Furthermore, by putting this cavity inside the vacuum chamber itself, it would allow us to get higher photon gains as the photon population within the resonator increases. To sum it up, while the laser is truly important for the entire process of accomplishing the experiment, this was indeed a mere step in allowing us to measure the fundamental constants better. After moving through these several hurdles, the experiment will allow us to measure the responses with a better clock than before.

Appendix A

Agilent 4433B

Here, all of the protocols/data you might want about Agilent 4433B would be placed here.

A.1 Labview and GPIB stuff

The connection from Agilent to the desktop was not too bad if you used Prologix GPIB-ETHERNET. Do not use NI-100 as the driver for that has been outmoded and no longer works (I have heard Michael might have gotten it to work but I am not sure of the details). The IP address was set to 10.1.2.1 last time I have checked. The address should be set to 22, but if it doesn't work, either change the code in Labview or change it in the function generator instead.

The code hacked up for the control of it is simple but it's probably worth a quick mention for posterity reasons. It is a simple state machine composed of four states:

The intended method of operation would be to lock the laser using FALC after you finish initializing, once locked, run scan, where it will progress forward and stop, once stopped, mode hope to the next mode, then scan back, and continue on until you are done scanning for the region you want. While it would be great if this could be automated, due to FALC being an analog PID controller, digital controls, without

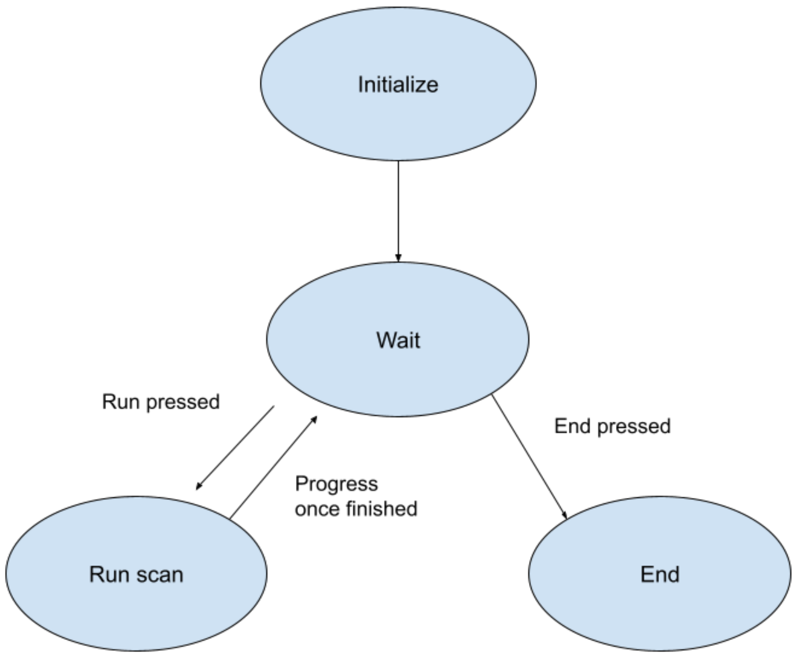

Figure A.1: Initialize will turn on the machine and set the frequency to its default start value (controlled at beginning of running) and will initialize everything. Wait is just stuck there until you press one of two buttons: run and stop. Scan will, as the name implies, run scan. All of the actual communication with Agilent happens inside a single box so just edit that, the scan will go up and down to hold the lock properly. End will turn off the outputs and gets itself into sleep mode.

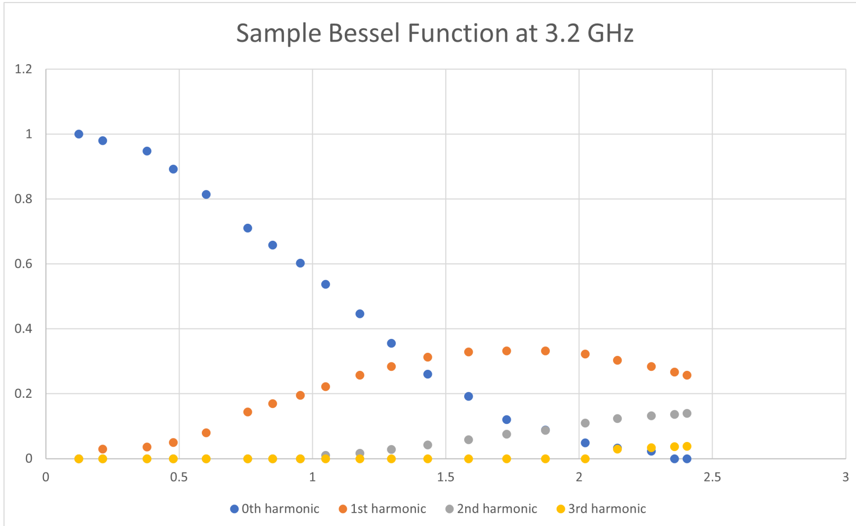

Figure A.2: As expected, the EOM exhibits an bessel squared response (the squared comes from the fact that this is measured with a photodiode) as the FM deviation changes.

extensive tinkering, would not be possible at the moment.

A.2 Unexpected Dips

The power curves for the signal generator consistently showed that there is a strong dip around 2.3 GHz. This indicates that the power leveling is faulty in the region of 2.3 GHz for both signal generators. Additionally, the machine is able to take on an external input for its frequency modulation, but it is only rated to the limits of 10 MHz. Anything beyond that may work, but will suffer from poorer SNR. If the need arises (for example, if you need to have a wider capture range), run it but add an additional gain to overcome the low pass filter that is applied to your signal (just a standard RC slope of -20 dB/decade).

A.3 Hopefully, Notes That Will Never Be Used

Hopefully nobody in the future will ever have to read this, but archiving things never truly hurt. The method of diagnosis will be that the machine will turn on, but no output will come out of it. The machine may even read that its leveling is broken. This occurs to the relay section after the oscillator being broken; however, due to the circuit being a precision, microwave circuit, fixing this would probably be futile. What is possible is to get the card for that section from elsewhere, but if what Professor Hall said is true, this is not the first time Agilent signal generators around this time broke for no good region (in the same place as well). If the machine does break, know that there is an output at the back that allows you to test the oscillator itself and you can use that in a pinch. It is typically covered up so you will have to unscrew it.

Bibliography

[1] W. M. Itano and N. F. Ramsey, "Accurate measurement of time," Scientific American **269**, 56–65 (1993).

[2] S. A. Diddams, J. C. Bergquist, S. R. Jefferts, and C. W. Oates, "Standards of time and frequency at the outset of the 21st Century," Science **306**, 1318–1324 (2004).

[3] Y. Stadnik and V. Flambaum, "Can Dark Matter Induce Cosmological Evolution of the Fundamental Constants of Nature?" Physical Review Letters **115** (2015), ISSN 1079-7114, URL `http://dx.doi.org/10.1103/PhysRevLett.115.201301`.

[4] R. Lange, N. Huntemann, J. M. Rahm, C. Sanner, H. Shao, B. Lipphardt, C. Tamm, S. Weyers, and E. Peik, "Improved Limits for Violations of Local Position Invariance from Atomic Clock Comparisons," Phys. Rev. Lett. **126**, 011102 (2021), URL `https://link.aps.org/doi/10.1103/PhysRevLett.126.011102`.

[5] J. Kobayashi, A. Ogino, and S. Inouye, "Measurement of the variation of electron-to-proton mass ratio using ultracold molecules produced from laser-cooled atoms," Nature Communications **10** (2019), ISSN 2041-1723, URL `http://dx.doi.org/10.1038/s41467-019-11761-1`.

[6] D. Hanneke, B. Kuzhan, and A. Lunstad, "Optical clocks based on molecular

vibrations as probes of variation of the proton-to-electron mass ratio," (2020), 2007.15750.

[7] A. Hartman, "Two-Photon Vibrational Transitions in O2+," Amherst College Undergraduate Thesis (2022).

[8] W. Henshon, "Radiofrequency circuit design for ion trapping of O2+ molecules," Amherst College Undergraduate Thesis (2023).

[9] D. Lane, "Developing a Quantum Toolbox: Experiments with a Single-Atom Har- monic Oscillator and Prospects for Probing Molecular Ions," Amherst College Undergraduate Thesis (2017).

[10] R. A. Carollo, D. A. Lane, E. K. Kleiner, P. A. Kyaw, C. C. Teng, C. Y. Ou, S. Qiao, and D. Hanneke, "Third-harmonic-generation of a diode laser for quantum control of beryllium ions," Optics Express **25**, 7220 (2017), ISSN 1094-4087, URL http://dx.doi.org/10.1364/OE.25.007220.

[11] W. G. Nagourney, *Quantum Electronics for atomic physics* (Oxford University Press, 2010).

[12] S. B. E. A. and M. C. Teich, *Fundamentals of photonics* (Wiley, 1991).

[13] B. G. Streetman and S. K. Banerjee, *Solid state electronic devices* (Pearson Education Limited, 2016).

[14] D. E. Aspnes, S. M. Kelso, R. A. Logan, and R. Bhat, "Optical properties of AlxGa1-x As," Journal of Applied Physics **60**, 754 (1986), ISSN 0021-8979, https://pubs.aip.org/aip/jap/article-pdf/60/2/754/18605888/754_1_online.pdf, URL https://doi.org/10.1063/1.337426.

[15] A. E. Siegman, *Lasers* (University Science Books, 1983).

[16] pratheeb N.P, "hermite gaussian beam," https://www.mathworks.com/matlabcentral/fileexcha hermite-gaussian-beam (2024).

[17] E. D. Black, "An introduction to Pound–Drever–Hall laser frequency stabilization," American Journal of Physics **69**, 79 (2001), ISSN 0002-9505, `https://pubs.aip.org/aapt/ajp/article-pdf/69/1/79/10115998/79_1_online.pdf`, URL `https://doi.org/10.1119/1.1286663`.

[18] J. Livas, J. Thorpe, K. Numata, S. Mitryk, G. Mueller, and V. Wand, "Frequency-tunable pre-stabilized lasers for LISA via sideband locking," Classical and Quantum Gravity **26**, 094016 (2009).

[19] Z. Zhao, Z. Bai, D. Jin, Y. Qi, J. Ding, B. Yan, Y. Wang, Z. Lu, and R. P. Mildren, "Narrow laser-linewidth measurement using short delay self-heterodyne interferometry," Opt. Express **30**, 30600 (2022), URL `https://opg.optica.org/oe/abstract.cfm?URI=oe-30-17-30600`.

[20] G. Di Domenico, S. Schilt, and P. Thomann, "Simple approach to the relation between laser frequency noise and laser line shape," Applied Optics **49**, 4801 (2010).

[21] N. Bucalovic, V. Dolgovskiy, C. Schori, P. Thomann, G. Di Domenico, and S. Schilt, "Experimental validation of a simple approximation to determine the linewidth of a laser from its frequency noise spectrum," Applied Optics **51**, 4582 (2012).

[22] R. Carollo, A. Frenett, and D. Hanneke, "Two-Photon Vibrational Transitions in 16O2+ as Probes of Variation of the Proton-to-Electron Mass Ratio," Atoms **7**, 1 (2018), ISSN 2218-2004, URL `http://dx.doi.org/10.3390/atoms7010001`.